025921-28-T

Semiannual Progress Report

National Aeronautics and
Space Administration
Ames Research Center
Moffett Field CA 94035

Pacific Missile
Test Center
Pt. Mugu CA
93042-5000

February 1992

THE UNIVERSITY OF MICHIGAN
Radiation Laboratory
Department of Electrical Engineering
and Computer Science
Ann Arbor, Michigan 48109-2122
USA

TECHNICAL REPORT

for NASA Grant NAG-2-541

NASA Technical Monitor: Alex Woo

Grant Title:	Development of 3D Electromagnetic Modeling Tools for Airborne Vehicles
Report Title:	Semiannual Progress Report
Institution:	Radiation Laboratory Department of Electrical Engineering and Computer Science The University of Michigan Ann Arbor MI 48109-2122
Period Covered:	September 1991 – February 1992
Principal Investigator:	John L. Volakis Telephone: (313) 764-0500

Table of Contents

Objective

Currently no software simulations are available from industry or academia which can allow an accurate computation of the radar signature from full scale non-metallic vehicles primarily because existing formulations have excessive memory and computational demands in addition to being unsuitable for modern machine architectures. Such software are required for test and evaluation purposes of future aircraft systems/platforms, target simulation platforms, on-board communication systems and for radar signature evaluation.

Traditional methodologies for radar signature or performance analysis of on-board communication systems have not shown any promise in simulating large scale composite vehicles. Furthermore, approximate simulation techniques are of no utility in modeling complex, composite structures. The intent of this research is thus aimed at developing new methodologies which will allow accurate and efficient simulations of full scale vehicles. We propose to accomplish this with the development of algorithms which have very low memory requirements and make use of recent advances in high performance and parallel computing. The particular technique to be employed is a hybrid version of the finite element method which has been successfully implemented and tested at the University of Michigan for two-dimensional applications. Also, some three dimensional results relating to specific scattering and antenna configurations have verified our expectations of the method's potential. The basis of this approach is to reformulate an open-boundary problem into a closed-boundary one using a mesh termination method which brings the outer boundary very close to the body. Segmentation and connectivity schemes can then be employed to subdivide the system/volume into smaller (of any number) sections which can be independently treated by separate single or parallel processors. Except for the small Toeplitz connectivity matrices, all others are sparse and banded, making their solution convenient, and since there is no need for concurrent storage of any of these submatrices, there is no limitation on the size of the computational domain, a problem which has become the bottleneck in computational electromagnetics. It is thus our claim that this solution approach, coupled with the advantages of the finite element method, will make a dramatic impact in the field of numerical electromagnetics, and promises to provide the necessary future tools for numerous applications, including target simulation, radar signature analysis and imaging, antenna modeling and VLSI circuit simulations.

Progress

As stated above, the main goal of this project is to develop methodologies for scattering by airborne composite vehicles. Although our primary focus continues to be the development of a general purpose code for analyzing the entire structure as a single unit, a number of other tasks are also pursued in parallel with this effort. These tasks, are important in testing the overall approach and in developing suitable models for materials coatings, junctions and, more generally, in assessing the effectiveness of the various parts comprising the final code.

Below we briefly discuss our progress on the five different tasks which were pursued during this period. Our progress on each of these tasks is described in the four detailed reports (025921-24-T, 025921-25-T, 025921-26-T, 025921-27-T) and the memoranda included with this document. The first task described below is, of course, the core of this project and deals with the development of the overall code. Undoubtedly, it is the outcome of the research which was funded by NASA-Ames and the Navy over the past three years.

Task: Three-dimensional hybrid finite element formulation for scattering

During this period we reached an important milestone in the development of the proposed electromagnetic tools. Specifically a full three dimensional code has been written and validated for computing the scattering by open bodies having arbitrary shape and material parameters. The completion of this code required the successful development of several new theoretical and mathematical procedures. Most importantly, a new mesh termination scheme was established to ensure the outgoing nature of the waves. With this scheme, the termination boundary was placed very close to the target thus greatly minimizing the unknown count. Moreover, the interior region was discretized with a new set of edge-based finite elements which do not suffer from the instabilities of the traditional node-based elements. By virtue of the employed near neighbor finite element method, the resulting system is sparse and when solved via an iterative method it has minimal memory requirements. We have so far solved systems having an unknown count of over 200,000 and our goal in the next few months is to increase the system size to more than 500,000. A major effort has also be devoted in establishing pre and post processing software and interfacing these with the new analysis code. As of the moment, we have interfaced our codes we a major commercial geometry/mesh generation package and several color

graphics tools and GUI platforms for entering and displaying the input and output data. More information on this task are provided in the University of Michigan technical report 0259121-24-T entitled "Application of Edge-Based Finite Elements and Vector ABCs in 3D Scattering." Representative results extracted from this report are shown in figures 1 and 2. These correspond to a metallic cube and circular cylinder, respectively.

Task: Improvements of the hybrid finite element method for a body of revolution

Last year a new finite element-boundary integral formulation for a body of revolution (BOR) was developed and coded as described in the University of Michigan technical report 025921-18-T. The developed formulation was superior from others in being capable of analyzing bodies with material coatings and inhomogeneous sections. In addition, by virtue of the formulation, only O(n) storage was required, important for large scale computations. However, it soon became apparent that the developed code was unsuitable for large bodies because of resonance conditions associated with the discrete system. The resonance characteristics are due to the boundary integral and have been a perennial difficulty to all formulations which make use of this integral. During this period we investigated several new method for eliminating these resonances and improving the efficiency of the code.

First, a new absorber termination (ATB) scheme was developed to replace the boundary integral (see figure 3). This approach leads to fully sparse matrices and is inherently rid of the resonances. However, the ATB had to be placed more than 1/2 wavelengths away from the structure, thus compromising the efficiency of the solution. At the moment we are investigating improvements to the ATB to be reported during the next period.

A second method for eliminating the resonances involved a recasting of the boundary integral with the scattered (rather than the total) field as the unknown. This approach is quite successful as illustrated in figure 4 for eliminating the resonances in two dimensions and is currently being implemented for three dimensional computations.

A third approach based on the implementation of a "complexification" scheme was also found equally successful in eliminating the resonances. This approach is attractive because of its simplicity. More details on its

implementation will be reported during the next period along with results and a description of the final code.

Additional details on our progress pertaining to this task are given in the University of Michigan technical report 025921-26-T.

Task: Resistive card modeling in the context of finite element solutions

Resistive cards are nowadays used on many airborne vehicles for radar cross section control. It is thus important to provide appropriate models for resistive cards in the context of the finite element method which is the basis of our methodology. The difficulty with traditional modeling of resistive cards is the implementation of the jump condition on the field across the sheet. This requires the specification of double nodes at the location of each resistive sheet, resulting in cumbersome and somewhat inefficient formulations. To avoid the double node specification, we modified the functional which is normally minimized in the implementation of the finite element method. The new functional does not require the specification of double nodes at the location of the resistive sheet, making it attractive to use in conjunction with commercial mesh generation packages. The new functional was tested and implemented in the new code described in the first task above. Details of the formulation are discussed in the University of Michigan report 025921-27-T.

Task: New finite element formulations and mesh termination schemes

In parallel with the development of the above more traditional hybrid finite element formulation and associated code we are also exploring new methods of implementation. The goal with these new implementations is efficiency, accuracy and simplicity. For example, in order to increase the efficiency of the solution we have considered new expansion functions and shapes of elements with the intent of using different expansion functions within a single mesh. The idea of this implementation is to provide the formulation with as much apriori information as possible, thus reducing the computational intensity and unknown count without comprising accuracy and geometrical adaptability. For this purpose, a two dimensional code was written which may break up the computational domain in different regions depending on the expected field complexity in those regions. Those regions over flat surfaces which are dominated by

geometrical optics fields can be modeled with large size elements and field shape functions which include in their representation the known geometrical optics or PTD fields. Small correction terms can then be introduced to provide the complete expression for the field in those regions.

Furthermore, to remove the requirement of a boundary integral for terminating the mesh we have separately explored the possibility of alternative mesh terminations schemes. The employed idea relies on the use of artificial absorbers placed in the near proximity of the body. The advantage of these absorbers is that they retain the sparsity of the matrix and this is crucial in reducing the computational intensity and memory requirement of the method. We have already developed and tested such absorbers (ATBs) and we continue to improve their absorptive properties to bring them as close to the body as possible without comprising accuracy.

Some of the details pertaining to this task are given in the included memorandum by D.C. Ross and J.L. Volakis dated January 5, 1992.

Task: Applications of wavelets to electromagnetics

Wavelets are a family of basis functions which are generated by translation and dilation of a single function. In the past they have been used for compressing data or functions defined over a large range. This is done by weighting/integrating or otherwise transforming the data with each of the basis in the wavelet family, thus generating an new array of data which is referred as the wavelet transform of the original data or function. The attractive property of the wavelet transform is its bandlimited form. This is because through inverse transformation each of the wavelet basis or functions adds details to the original function that are sequentially ordered in accordance with their level of importance. More on the fundamentals of this property is described in the attached memorandum by L.C. Kempel. In this memorandum an application of wavelets to electromagnetics is described. In particular the wavelet transform is instead applied to a large complex matrix resulting from the discretization of a typical boundary integral. By application of the wavelet transform, it is shown that a full matrix can be compressed to a banded matrix, important for reducing the solution's memory requirements. The included memorandum is a preliminary study and additional applications are planned in the next few months. The goal is to take advantage of the wavelet transform in treating the boundary integral matrix arising in some hybrid finite element formulations.

Task: Alternative integral equations for scattering by three dimensional coated structures

Thin material coatings are nowadays routinely used in the construction all airborne vehicles. Nevertheless, their electromagnetic characterization in the context of integral equations still relies on the use of the simple but less accurate impedance boundary conditions. On the other hand, although finite element formulations can readily deal with the presence of material coatings, their implementation is inefficient when the coating becomes thin. This is because very small elements must be used in the vicinity of the thin coating.

To avoid the inaccuracy of the impedance boundary condition and the inefficiency of the finite element method for modeling thin coatings, a new integral equation was derived and discretized for implementation. The derivation of the new integral equation is described in the University of Michigan technical report 025921-25-T entitled "Alternative field representations and integral equations for modeling inhomogeneous dielectrics." In comparison with traditional integral equations which require as many as eight unknowns in their discretization, the new integral equations requires only three unknowns per cell without any compromise in accuracy. The approximate integral equation based on the impedance boundary condition requires four unknowns per cell. In addition the new integral equation is also associated with a lower kernel singularity which greatly facilitates its discretization. A code based on this formulation is currently being written and results based on this code will be reported during the next few months.

Task: New impedance wedge diffraction coefficients

Sometime ago we reported in the University of Michigan report 025921-4-T a new approximate impedance wedge diffraction coefficient for characterizing the diffraction by an impedance wedge. We resorted to an approximate coefficient only because the impedance wedge is not amenable to an exact solution when excited by a wave incident in a plane other than that normal to the wedge. This diffraction coefficient was later implemented and successfully tested in a traditional PTD code under a contract supported by the U.S. Army (see University of Michigan report 028371-1-F).

After several applications, the aforementioned diffraction coefficient was found to be at times inaccurate for computing the cross polarization fields. To remedy this deficiency, we examined the possibility of a more rigorous development for the proposed diffraction coefficients. From the start, this effort proved challenging but we have now arrived at a procedure which has yielded a more accurate diffraction coefficient. The new coefficient is still under testing and will be reported in an upcoming technical report. Also based on this diffraction coefficient, we shall derive new equivalent currents for possible implementation in a PTD code.

Transitions

During the next period we shall emphasize the following

1. The application of the developed finite element-ABC code for scattering computations associated with large composite bodies. The intended calculations should prove the method's suitability for large scale implementations.

2. Develop a segmentation and/or connectivity scheme to subdivide the computational domain of the vehicle for parallel implementations. This approach should facilitate the discretization of large size structures and computations associated with full scale vehicles.

3. Develop improved absorber termination schemes (ATBs) for terminating the finite element mesh as close to the structure as possible.

4. Examine the viability of a new hybrid high frequency-finite element method. This approach is intended to reduce the unknown count and thus increase the computational efficiency of the method.

5. Complete the development of the improved finite element-boundary integral BOR code. As noted earlier, the new code will be rid of difficulties associated with the internal body resonances.

6. Complete and validate the code based the new integral equation for coated bodies.

7. Complete the development and test the accuracy of the new skew incidence impedance wedge diffraction coefficient.

List of reports submitted this period

A. Chatterjee, J.M. Jin, and J.L. Volakis, "Application of edge-based finite elements and vector ABCs in 3D scattering," Univ. of Michigan Radiation Laboratory Report #025921-24-T, Jan. 1992.

J.L. Volakis, "Alternative field representations and integral equations for modeling inhomogeneous dielectrics," Univ. of Michigan Radiation Laboratory Report #025921-25-T, Feb. 1992.

J.D. Collins and J.L. Volakis, "Progress on hybrid finite element methods for scattering by bodies of revolution," Univ. of Michigan Radiation Laboratory Report #025921-26-T, Feb. 1992.

J.M. Jin, J.L. Volakis, C.L. Yu and A.C. Woo, "Modeling of resistive sheets in finite element solutions," Univ. of Michigan Radiation Laboratory Report #025921-27-T, Feb. 1992.

Semiannual Progress Report for NASA Grant NAG-2-541, "Development of 3D Electromagnetic Modeling Tools for Airborne Vehicles," Univ. of Michigan Radiation Laboratory Report #025921-28-T, Feb. 1992.

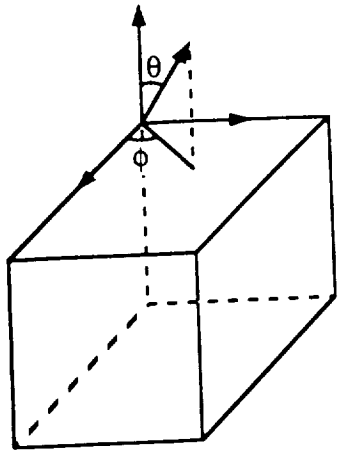

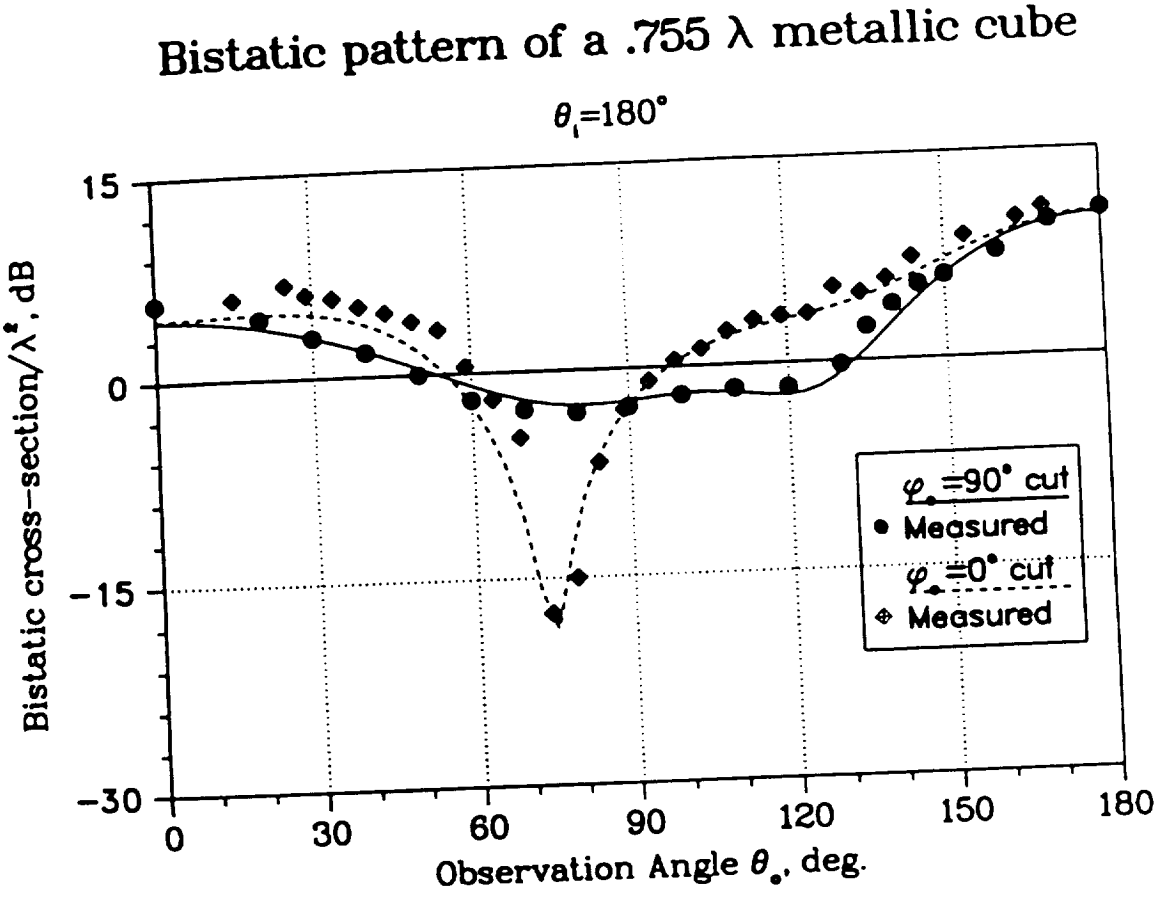

Figure 1: Bistatic pattern ($\theta_i = 180°$) of a metallic cube having an edge length of 0.755λ using the 2nd order vector absorbing boundary condition.

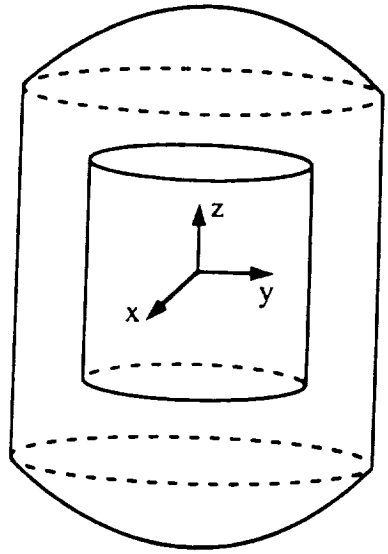

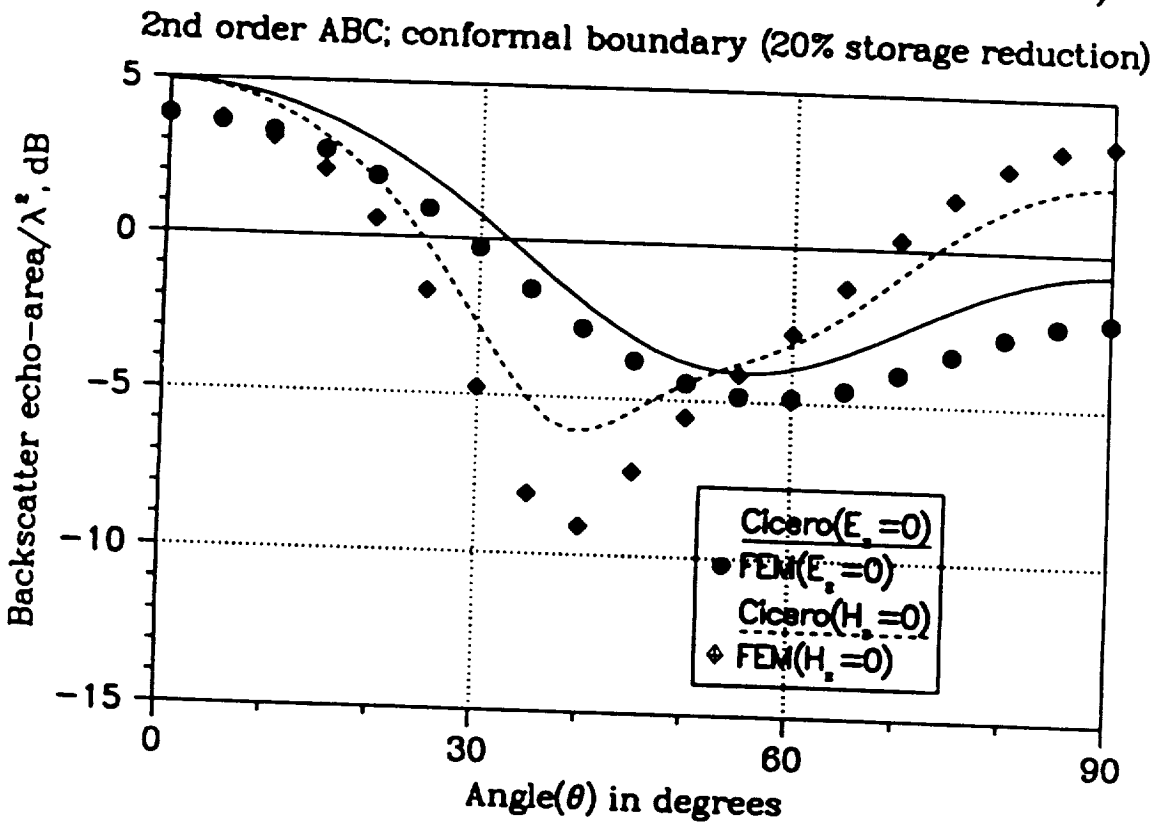

Figure 2: Backscatter pattern of the cylinder in Figure 7 enclosed by a conformal outer boundary and using the second order absorbing boundary condition.

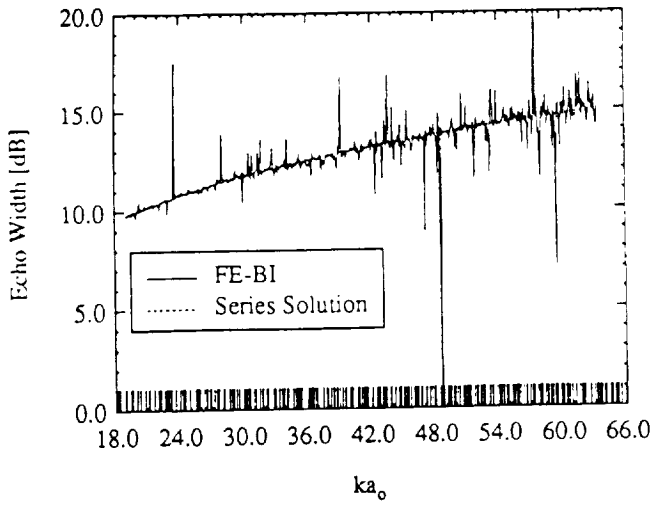

(a)

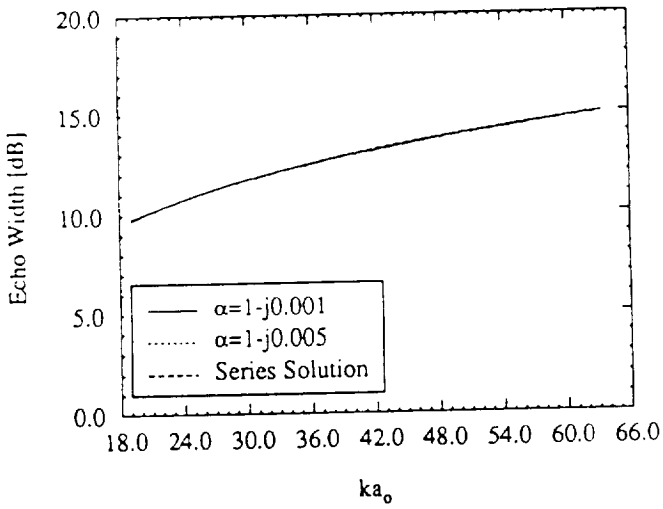

(b)

Figure 3: Backscattering echowidth of a circular cylinder: (a) original formulation; (b) scattered field formulation with complexification.

Memorandum 1

A Finite Element Formulation for Scattering from Electrically Large 2-Dimensional Structures.

Daniel C. Ross and John L. Volakis

January 5, 1992

***Abstract*—A Finite Element Formulation is given using the scattered field approach with a fictitious material absorber to truncate the mesh. The formulation includes the use of arbitrary approximation functions so that more accurate results can be achieved without any modification to the software. Additionally, non-polynomial approximation functions can be used, including complex approximation functions. The banded system that results is solved with an efficient sparse/banded iterative scheme and as a consequence, large structures can be analyzed. Results are given for simple cases to verify the formulation and also for large, complex geometries.**

I. Introduction

The popularity of the Finite Element Method (FEM) in Electromagnetic Scattering is largely due to the fact that the method results in a banded system with an $O(N)$ memory demand. This is in sharp contrast to the Moment Method which has an $O(N^2)$ memory demand. For open region scattering problems however, the Finite Element region must be artificially truncated in order to bound the problem. This has been accomplished with approximate methods such as the Uni-Moment Method [1] and the Absorbing Boundary Condition [6] and more successfully with the rigorous Boundary Integral Technique [3]. Unfortunately, the solution of the Boundary Integral in general results in a dense system thus destroying the $O(N)$ character of the FEM. Also, the boundary integral technique breaks down at resonant frequencies and these resonant frequencies become more and more closely spaced as the size of the boundary is increased.

More recently, the technique of using a fictitious material absorber to confine the scattered field has been suggested in [4]. Since fictitious materials having a negative real part of μ and ϵ can be used, an absorber with a very low reflection coefficient even at near grazing incidence can be realized. Also, this technique requires the unknown quantity to be the scattered field, not the total field as is usually the case. The benefits of this are two-fold. First, the scattered field does not vary as rapidly as the total field and second, the scattered field approach requires that the incident field be evaluated in the interior of the mesh, thus reducing the phase error

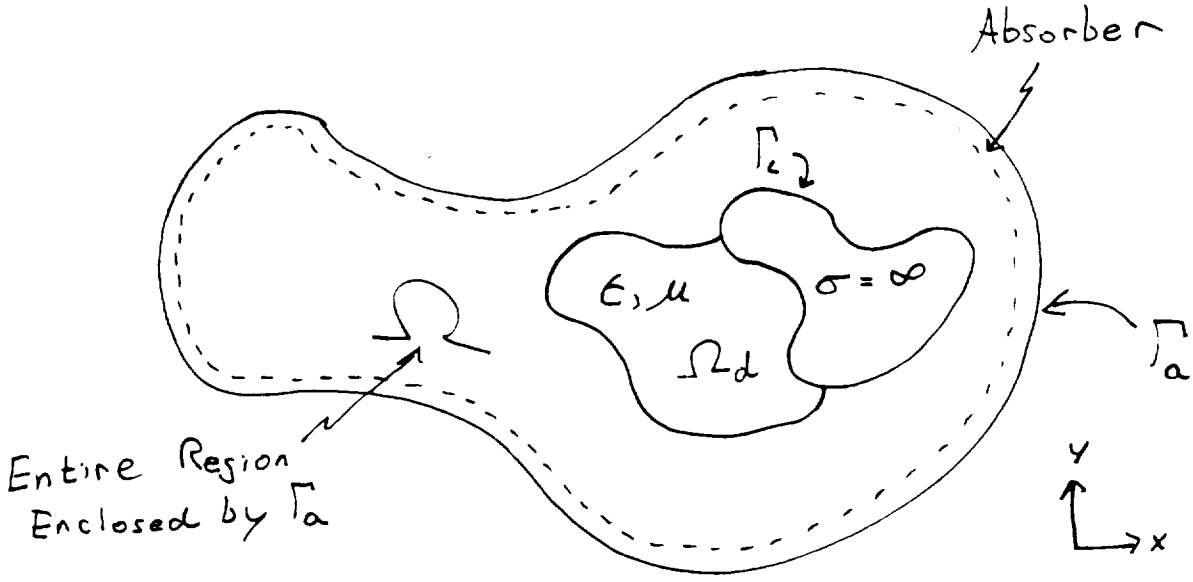

Figure 1: Region of solution

normally associated with the total field approach. That is, the total field approach requires that the incident field be evaluated only at the fictitious boundary and then propagate through the mesh to the scatterer thus introducing phase error, especially notable when the mesh is large. It has been confirmed in [5] that the scattered field approach results in a more accurate solution.

It is known that there is also an overall inherent error in the FEM that does not exist in the Moment Method [7]. This error is a result of the bandedness of the system and is introduced as the solution propagates through the mesh. In fact, experience has shown that as the mesh area increases, the element size must decrease. The only solution to this problem is to use higher order approximation functions, which usually involves a complete re-formulation and re-design of the software.

In this paper a number of advances in FEM calculations are combined to give a solution to the 2-Dimensional Helmholtz equation for electrically large scatterers. The scattered field approach is used and a fictitious material absorber is used to truncate the mesh. Unique to this formulation is the use of arbitrary approximation functions that make it possible to increase the accuracy of the solution without modifying the software.

II. Formulation

Consider the region shown in Figure 1.

Given that there is some incident field, we wish to solve the wave equation in the region Ω and find the fields scattered by the dielectric/magnetic/conducting target.

The source free wave equation in two dimensions can be written

$$\nabla \cdot (u \nabla \phi) + k_0^2 v \phi = 0 \tag{1}$$

where

$$\phi = E_z \tag{2}$$
$$u = 1/\mu_r \tag{3}$$
$$v = 1/\epsilon_r \tag{4}$$

for E polarization (z directed electric field)

and

$$\phi = H_z \tag{5}$$
$$u = 1/\epsilon_r \tag{6}$$
$$v = 1/\mu_r \tag{7}$$

for H polarization (z directed magnetic field)

Now let T be some compactly supported testing function used to enforce (1) over the entire region.

$$\iint_\Omega T[\nabla \cdot (u \nabla \phi) + k_0^2 v \phi]\, ds = 0 \tag{8}$$

Using the identity

$$T[\nabla \cdot (u \nabla \phi)] = -u(\nabla \phi \cdot \nabla T) + \nabla \cdot (T u \nabla \phi) \tag{9}$$

gives

$$\iint_\Omega [u(\nabla T \cdot \nabla \phi) - k_0^2 v T \phi]\, ds - \iint_\Omega \nabla \cdot (T u \nabla \phi)\, ds = 0 \tag{10}$$

and applying the divergence theorem to the second term in the above brings us to the weak form of eqn. (1).

$$\iint_\Omega [u(\nabla T \cdot \nabla \phi) - k_0^2 v T \phi]\, ds - \oint_{\Gamma_a} uT \frac{\partial \phi}{\partial n}\, d\ell - \oint_{\Gamma_c} uT \frac{\partial \phi}{\partial n}\, d\ell = 0 \tag{11}$$

To use eqn. (11) in an FEM implementation would be considered a total field approach since the unknowns would be the total field. To get the analog of (11) with the scattered field as the unknown we let

$$\phi = \phi^s + \phi^i \tag{12}$$

and (11) becomes

$$\iint_\Omega [u(\nabla T \cdot \nabla \phi^s) - k_0^2 v T \phi^s]\, ds - \oint_{\Gamma_a} T(u\frac{\partial \phi^s}{\partial n} + \tilde{u}\frac{\partial \phi^i}{\partial n})\, d\ell \tag{13}$$
$$- \oint_{\Gamma_c} T(u\frac{\partial \phi^s}{\partial n} + \tilde{u}\frac{\partial \phi^i}{\partial n})\, d\ell = - \iint_\Omega [\tilde{u}(\nabla T \cdot \nabla \phi^i) - k_0^2 \tilde{v} T \phi^i]\, ds$$

where $\tilde{u}$ and $\tilde{v}$ are the material constants of the scatterer in a free space environment while u and v include the fictitious absorber. In this way the incident field does not interact with the fictitious absorber.

In either case, eqns. (11) and (13) require that the normal derivative of the unknown (total field and scattered field respectively) be specified on the enclosing boundaries Γ_a and Γ_c. These normal derivatives are arbitrary, and once given, a solution in the interior is uniquely defined.

For E polarization we will put a perfect magnetic conductor at Γ_a and for H polarization we will put a perfect electric conductor at Γ_a thus the second term on the LHS of (13) is

$$- \oint_{\Gamma_a} \tilde{u} T \frac{\partial \phi^i}{\partial n}\, d\ell \tag{14}$$

Note that this conductor is seen by the scattered field only, not the total field.

The boundary condition at Γ_c is

$$\frac{\partial \phi^s}{\partial n} + \frac{\partial \phi^i}{\partial n} = 0 \tag{15}$$

for H polarization, and thus the third term on the LHS of (13) is zero.

For E polarization the boundary condition at Γ_c is

$$\phi^s + \phi^i = 0 \tag{16}$$

and since the solution is specified on this contour, the normal derivatives will uncouple from the rest of the equation once we have discritized (13) and created a linear system, thus the third term on the LHS of (13) drops out.

We have that eqn. (13) becomes

$$\iint_\Omega [1/\mu_r(\nabla T \cdot \nabla \phi^s) - k_0^2 \epsilon_r T \phi^s]\, ds - \oint_{\Gamma_a} 1/\tilde{\mu}_r T \frac{\partial \phi^i}{\partial n}\, d\ell = \tag{17}$$
$$- \iint_\Omega [1/\tilde{\mu}_r(\nabla T \cdot \nabla \phi^i) - k_0^2 \tilde{\epsilon}_r T \phi^i]\, ds$$

for E polarization and

$$\iint_\Omega [1/\epsilon_r(\nabla T \cdot \nabla \phi^s) - k_0^2 \mu_r T \phi^s]\, ds - \oint_{\Gamma_a} 1/\tilde{\epsilon}_r T \frac{\partial \phi^i}{\partial n}\, d\ell = \tag{18}$$
$$- \iint_\Omega [1/\tilde{\epsilon}_r(\nabla T \cdot \nabla \phi^i) - k_0^2 \tilde{\mu}_r T \phi^i]\, ds$$

for H polarization.

The region Ω now is divided into arbitrary, polygonal finite elements. Each element is defined by its corner nodes and may contain other nodes located anywhere in the element. The solution in the e'th element is approximated by

$$\phi^e(x,y) = \sum_{n=1}^{N^e} S_n^e(x,y)\phi_n^e \tag{19}$$

where N^e is the total number of nodes in the e'th element, ϕ_n^e is the value of ϕ at the n'th node and $S_n^e(x,y)$ is the n'th shape function for the e'th element understood to be zero outside of the e'th element. These shape functions will be defined in the next section. To solve (17) and (18) using Galerkin's method, we let the testing function T be the same as the basis function in (19).

Substituting (19) into (17) and (18) gives the Element Equations

$$\iint_{\Omega_e} [1/\mu_r^e \nabla S_i^e \cdot \nabla \sum_{j=1}^{N^e} S_j^e \phi_j^e - k_0^2 \epsilon_r^e S_i^e \sum_{j=1}^{N^e} S_j^e \phi_j^e]\, ds = \tag{20}$$

$$+ \oint_{\Gamma_e} 1/\tilde{\mu}_r^e S_i^e \frac{\partial \phi^i}{\partial n}\, d\ell - \iint_{\Omega_e} [1/\tilde{\mu}_r^e (\nabla S_i^e \cdot \nabla \phi^i) - k_0^2 \tilde{\epsilon}_r^e S_i^e \phi^i]\, ds \quad i = 1,2,3...N$$

for E polarization and

$$\iint_{\Omega_e} [1/\epsilon_r^e \nabla S_i^e \cdot \nabla \sum_{j=1}^{N^e} S_j^e \phi_j^e - k_0^2 \mu_r^e S_i^e \sum_{j=1}^{N^e} S_j^e \phi_j^e]\, ds = \tag{21}$$

$$+ \oint_{\Gamma_e} 1/\tilde{\epsilon}_r^e S_i^e \frac{\partial \phi^i}{\partial n}\, d\ell - \iint_{\Omega_e} [1/\tilde{\epsilon}_r^e (\nabla S_i^e \cdot \nabla \phi^i) - k_0^2 \tilde{\mu}_r^e S_i^e \phi^i]\, ds \quad i = 1,2,3...N$$

for H polarization.

Again, $\tilde{\mu}_r^e$ and $\tilde{\epsilon}_r^e$ are the material constants of the scatterer in a free space environment while μ_r^e and ϵ_r^e include the fictitious absorber.

Equations (20) and (21) define an N^e by N^e linear system for a single element. Assembling all of the element systems together and converting to global node numbers gives the global finite element system

$$[K]\{\phi^s\} = \{\Phi^i\} \tag{22}$$

For E polarization only, the boundary condition (16) must be enforced by setting $\phi^s = -\phi^i$ for nodes on the conductor.

III. Arbitrary Approximation Functions

In eqn. (19) the expansion of the solution was given as a sum of N shape functions weighted by the nodal values of the solution. To determine these shape functions let

$$\phi^e(x,y) = \sum_{n=1}^{N^e} a_n f_n(x,y) \tag{23}$$

where the $f_n(x,y)$'s are linearly independent functions known as approximation functions.

Forcing $\phi^e(x,y)$ to be $\phi_i^e(x_i,y_i)$ at each nodal point gives the system

$$[F_{ij}^e]\{a_i^e\} = \{\phi_i^e\} \tag{24}$$

where $[F_{ij}^e]$ is an N by N matrix whose i,j'th element is given by $f_j(x_i,y_i)$ and x_i,y_i are the coordinates of the i'th node. For ease of programming, these approximation functions are often chosen to be linear, ie. $f_1 = 1, f_2 = x, f_3 = y$. However, since it is known that higher order approximation functions result in better conditioned systems and are more accurate[1], it is desirable to use approximation functions of arbitrary order or even of a non-standard type such as complex transcendental functions which are better suited for Electromagnetics.

The shape functions are then given by

$$S_n^e(x,y) = \sum_{i=1}^{N^e} f_i(x,y)[F_{in}^e]^{-1} \tag{25}$$

Notice that the first derivatives of the shape functions are also required and this must be taken into account when choosing approximation functions since from (23), derivatives of the shape function transfer directly to the approximation functions.

Note also that the inverse of an N^e by N^e matrix is required to calculate the shape function for each element. Since N^e will not be very large, this does not introduce any great expense.

When the arbitrary shape functions are used to generate the element matrices an efficient numerical integration scheme must be used. Since the elements are arbitrary polygons, an integration algorithm based on the polygon fill algorithm from computer graphics was developed. This integration algorithm takes as input: the number of points defining the polygon, the coordinates of these points, the number of sub-regions to split the area into, the order of the Gaussian quadrature to use, and the integrand function. With some experimentation, it was found that increasing the accuracy of the integrations had little effect on the far field scattering patterns once the integrations were approximately five percent accurate (for linear shape functions.)

IV. Results

The bistatic RCS pattern for a perfectly conducting circular cylinder of radius $\lambda/2$ is shown in figure 2. Linear shape functions were used and as can be seen from figure 3 a discretization of $\lambda/20$ was required. The fictitious absorber was placed $\lambda/2$ away from the cylinder to avoid interactions with the scatterer.

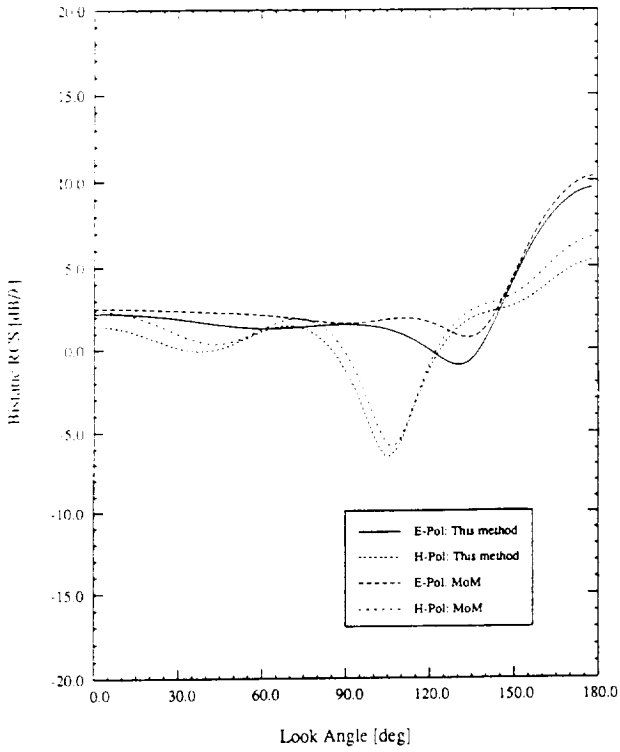

Figure 2: Bistatic RCS of conducting cylinder

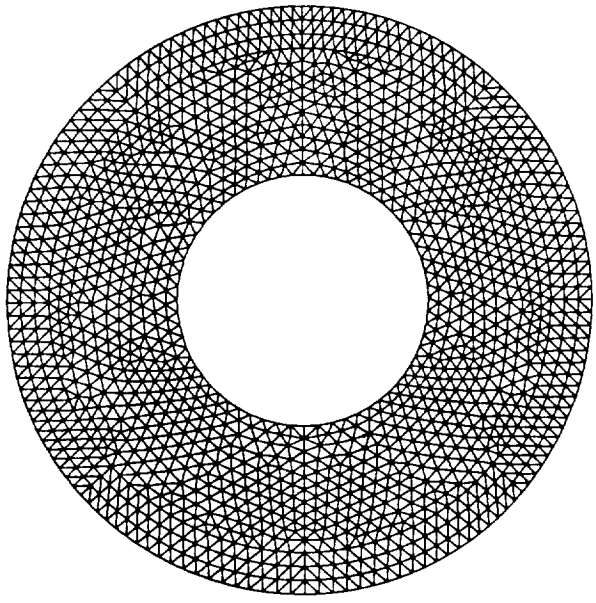

Figure 3: Mesh for $r = \lambda/2$ conducting cylinder

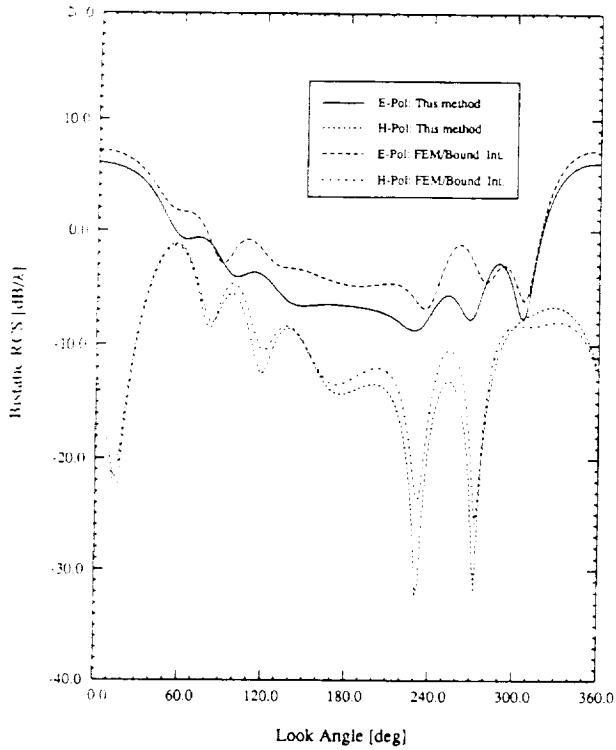

Figure 4: Bistatic RCS of Airfoil

A more useful result is shown in figure 4 for a perfectly conducting airfoil at low frequency. The wing is approximately $1\frac{3}{4}\lambda$ long and as can be seen from figure 5 a discretization of $\lambda/20$ was again required but the fictitious absorber needed to be placed a full wavelength away from the target in order to get accurate results for H polarization. The reason for the discrepancy in the E polarization results is that the artificial absorber actually needs to be placed farther away from the scatterer. The following discussion addresses this issue.

For quadratic shape functions, which are obtained by setting $f_1 = 1, f_2 = x, f_3 = y, f_4 = xy, f_5 = x^2$, and $f_6 = y^2$, the mesh is not as dense as can be seen from figure 6. However since there are twice as many nodes per element, the net effect is that there are about half as many elements but the same number of nodes. However the increase in accuracy makes it possible to analyze larger and more detailed scatterers.

For cubic shape functions, which are obtained by setting, for example, $f_1 = 1, f_2 = x, f_3 = y, f_4 = xy, f_5 = x^2, f_6 = y^2, f_7 = x^3, f_8 = y^3, f_6 = x^3y^3$, the mesh is even less dense as can be seen from figure 7. Again, there are approximately the same number of nodes but the number of elements is cut in half. Actually, since the accuracy is increased exponentially, the mesh size could be increased further thus actually reducing the number of unknowns. This would seem to imply that higher order approximation functions keep getting more efficient. Whether or not this is the case remains to be seen.

Another choice of approximation function could be the Hankel function of order 0. This would make it possible to discretize using larger elements far away from the scatterer where the wave becomes somewhat cylinderical. There would still be other approximation functions to allow

[1] Polynomial approximation functions of Order p result in a solution which is h^p accurate where h is the mesh size.

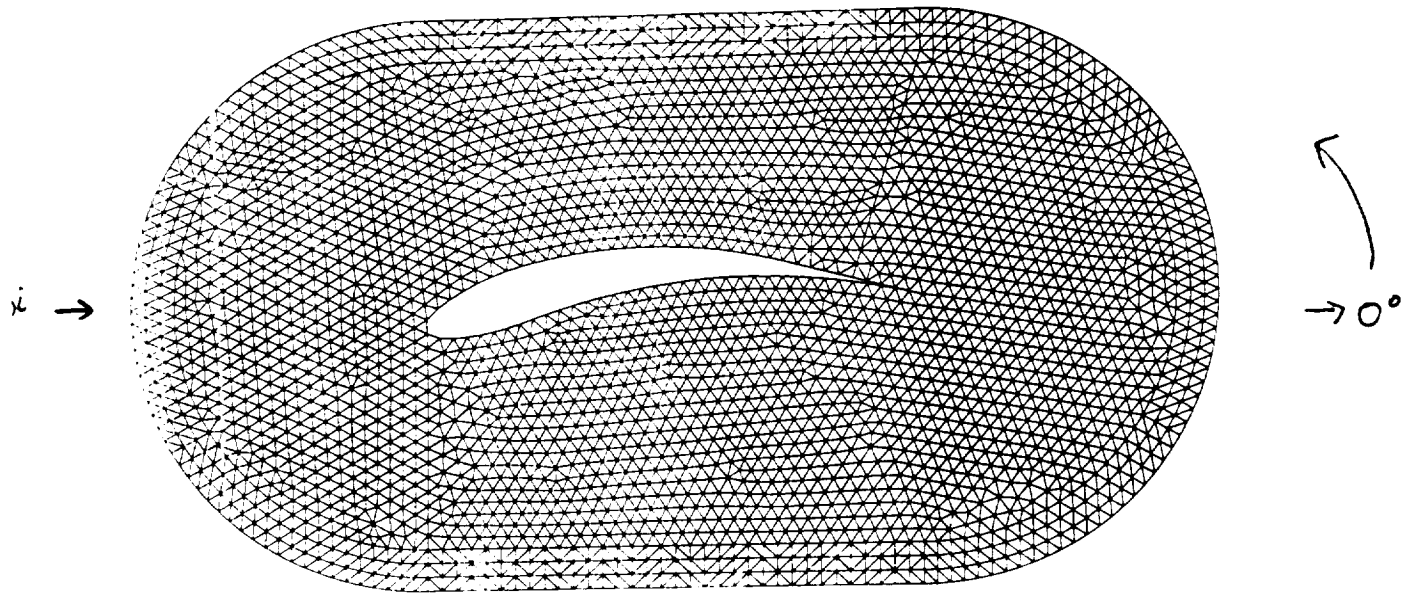

Figure 5: Mesh for Airfoil : Linear

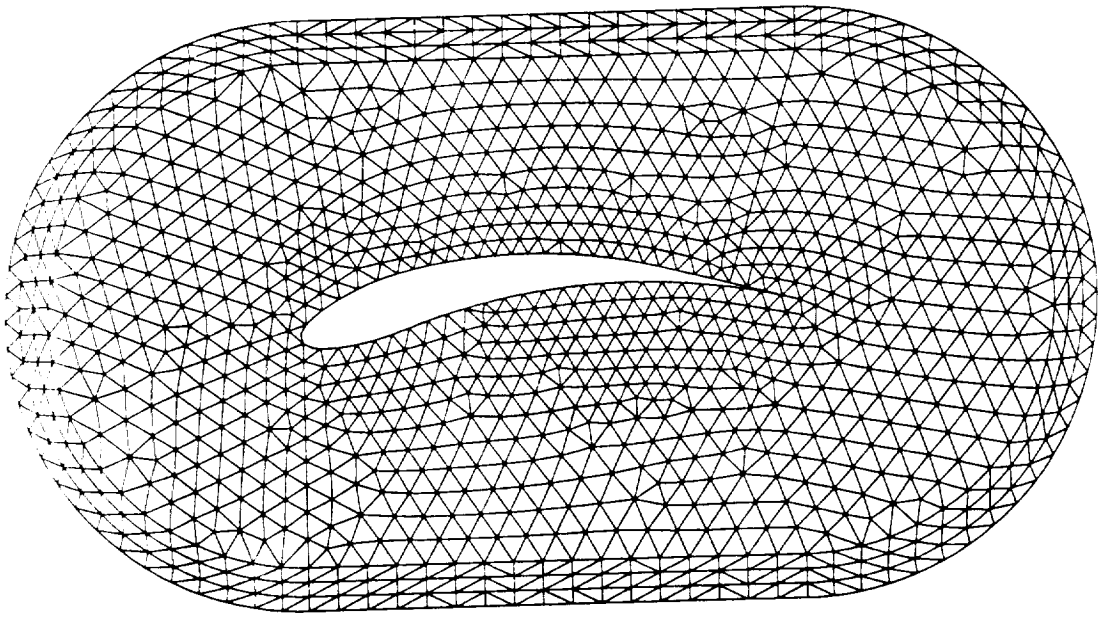

Figure 6: Mesh for Airfoil : Parabolic

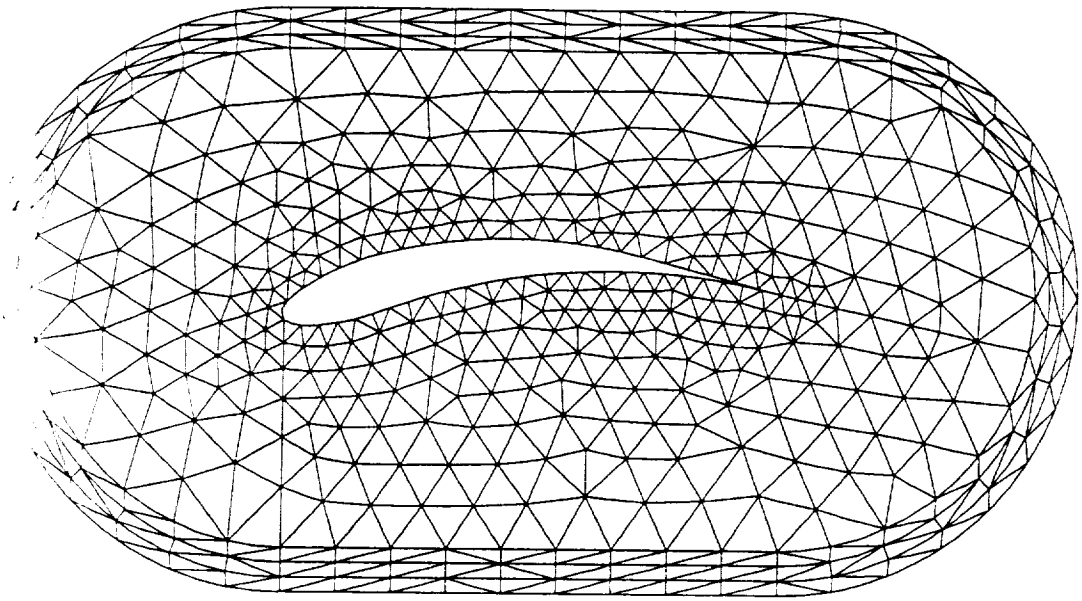

Figure 7: Mesh for Airfoil : Cubic

some modification to the cylinderical wave. Being able to efficiently discretize large regions is desirable since it is clear from the results for the airfoil that the artificial absorber must be placed far away from the scatterer. Actually, one could consider the transcendental Hankel function to be of exact accuracy limited only by numerical considerations. This is a feature that polynomial basis functions do not possess since they do not themselves solve the wave equation.

V. Conclusions

Although much more testing must be done with both the placement of the artificial absorber and the use of higher order and complex approximation functions, it is clear that this type of formulation holds promise for the accurate analysis of large scatterers. While many formulations are specific to a certain problem and do not allow for growth and modification, the above formulation and the software developed provide a flexible tool for improving the current state of FEM for the analysis of large electromagnetic scattering problems.

References

[1] Mei, K. K., "Unimoment Method of Solving Antenna and Scattering Problems," IEEE Transactions on Antennas and Propagation, AP-22, 760-766, 1974

[2] A. Bayliss, M. Gunzburger and E. Turkel, "Absorbing Boundary Conditions for the Numerical Solution of Elliptic Equations in Exterior Regions," SIAM J. Appl. Math., vol. 42, pp 430-451, April 1982.

[3] Jin and Volakis

[4] Jian-Ming Jin, John L. Volakis, and Valdis V. Liepa, "An Engineer's Approach for Terminating Finite Element Meshes in Scattering Analysis"

[5] Omar M. Ramahi and Raj Mittra, "Finite-Element Analysis of Dielectric Scatterers Using the Absorbing Boundary Condition," IEEE Transactions on Magnetics, Vol. 25, No. 4, pp 3043-3045, July 1989.

[6] Bayliss, A.,M. Gunzburger, and E. Turkel, "Boundary Conditions for the Numerical Solution of Elliptic Equations in Exterior Regions," SIAM J. Appl. Math., 42, 430-451, 1982

[7] Andrew F. Peterson and Richard J. Baca, "Error in the Finite Element Discretization of the Scalar Helmholtz Equation Over Electrically Large Regions," IEEE Microwave and Guided Wave Letters, Vol.1 No. 8, pp 219-222 August 1991.

Memorandum 2

Wavelets and Electromagnetics

Leo C. Kempel
Radiation Laboratory
Department of Electrical Engineering and Computer Science
University of Michigan, Ann Arbor, MI 48109-2122

December 19, 1991

Abstract

Wavelets are an exciting new topic in applied mathematics and signal processing. This paper will provide a brief review of wavelets which are also known as families of functions with an emphasis on interpretation rather than rigor. We will devise an indirect use of wavelets for the solution of integral equations based upon techniques adapted from image processing. Examples for resistive strips will be given illustrating the effect of these techniques as well as there promise in reducing dramatically the storage requirement in order to solve an integral equation for large bodies. We also will present a direct implementation of wavelets to solve an integral equation. Both methods suggest future research topics and may hold promise for a variety of uses in computational electromagnetics.

1 Introduction

Wavelets have generated significant excitement among applied mathematicians and engineers recently due to their unique properties and diversity. Wavelets are actually a family of basis functions which are generated by translation and dilation of a single function. The uses are diverse since many different wavelets may be generated which possess some properties which are particularly well suited for a given purpose. Three prominent uses of

wavelets are image compression which is discussed by Mallat([1],[2]) and Daubechies[3], solution of partial differential equations by the staff at Aware Inc.([4], [5]), and the solution of Fredholm Integral Equations by several members of the Yale research staff([6],[7],[8]).

This paper will give a brief and basic review of wavelets with an emphasis on the character of these functions rather than a rigorous mathematical treatment. Our purpose is to apply wavelet expansions or wavelet transforms to the solution of electromagnetic problems. We will show that a novel technique which is adopted from image processing may be applied to traditional Method of Moments(MoM) computer codes to achieve significant storage savings. Since modern computers are becoming increasingly fast, the primary limitation on MoM implementations is the $\mathcal{O}(N^2)$ storage requirement. The use of wavelets is intended to alleviate this requirement. This "image processing" technique may be used with existing MoM implementations to reduce storage. Finally we will look at direct applications of wavelets in electromagnetics with a modal solution of the Fredholm equation and discuss future research topics. Although we have only used E-polarized resistive strip examples for this paper these techniques are applicable to other electromagnetic problems of interest. In particular, although we only use MoM examples herein, we are interested in applying wavelet analysis in the solution of the boundary integral associated with the FEM-BE method.

2 Wavelets and Dilation Equations

Wavelets and their underlying form, a dilation equation, is an unfamiliar concept to most engineers. We will attempt to give a feel for what a wavelet is and what properties it possesses which are attractive for electromagnetics without going into detail. Strang[9] gave an excellent high-level review of the properties of wavelets while Daubechies[10] provides a rigorous review with significant new material. Mallat[2] was able to relate wavelet decomposition and reconstruction in terms of multiresolution analysis which allowed significant progress to be made in exploiting wavelets for the aforementioned applications.

In order to understand wavelets, we must first look at a dilation equation

$$\phi(x) = \sum_k c_k \phi(2x - k) \tag{1}$$

which is recognized as a two-scale difference equation. Strang[9] reviews the criterion which must be met in order for (1) to be unique. The "scaling function",$\phi(x)$, is determined recursively and thus many properties of it must be observed rather than defined. Daubechies[10] was able to construct orthonormal wavelets with compact support in both domains which was thought to be impossible by using the recursion

$$\phi_j(x) = \sum_k c_k \phi_{j-1}(2x-k) \tag{2}$$

with the box function as the fundamental function ($\phi_0(x)$) and certain simple conditions which determine c_k. The family of wavelets derived by Daubechies will be used for the examples of this paper although this is certainly not the only or necessarily optimal choice of wavelets.

At this point, we introduce the continuous wavelet family which comes from the scaling function,$\phi(x)$, as

$$\psi(x) = \sqrt{s}\phi(s(x-u)) \tag{3}$$

where the scale parameter(s) and the translation parameter(u) range over the positive real axis and the entire real axis, respectively (The notation adopted for the remainder of this paper is from Mallat [1]). A fundamental property of wavelets is their approximation capability. Daubechies family is denoted by the number of recursions used to determine the analyzing wavelet. For example we will denote the Daubechies wavelet which has four coefficients as DAUB4 which can recover up to a linear polynomial since the two lowest-order moment vanishes as discussed by Strang[9]. As terms are increased, more moments vanish and thus the polynomial approximation increases in order (e.g. DAUB6 will recover a quadratic).

As was previously mentioned, the Daubechies family is not only orthonormal but they enjoy the useful property of compact support. For example, figure 1 illustrates DAUB20 wavelet compared with the comparable cosine if we wish to represent an impulse "frequency" of $f = \frac{24}{1024\Delta}$ where Δ is the spatial sample size. As seen, the cosine(Fourier series basis) is compact in the "frequency" domain yet requires infinite support in the spatial domain. However, the Daubechies wavelet is compact in both domains. A further example is given in figure 2 where the excitation impulse is at $f = \frac{100}{1024\Delta}$ and we observe that as the "frequency" increases, the analyzing wavelet has

diminishing spatial support. This is the most important property of wavelets since finer spatial resolution is used for "high frequency" components which results in a more accurate evaluation than is possible for the comparable Fourier coefficient which is computed with constant sample size regardless of the "frequency".

Several groups ([4],[5],[6],[7], [8]) have recognized that the property of compact support in both domains will result in a sparse matrix when an integral operator is converted to a matrix operator. We will discuss in the next section the fact that if one thinks in terms of multiresolution analysis, the preceding observation is obvious.

3 Matrix Compression Techniques

One of the most promising applications of wavelets is image compression for the transmission and storage of detailed images. For example, The FBI is looking at using wavelet compression techniques in order to store their extensive finger print library without loss of fidelity. We will give a brief review of the wavelet transform, multiresolution analysis , and what this topic has to do with electromagnetics.

The continuous wavelet transform is given here without proof[1]

$$F(s,u) = \int_{-\infty}^{\infty} f(x)\psi_s(x-u)dx \tag{4}$$

where the wavelet family is given

$$\psi_s(x) = \sqrt{s}\psi(sx) \tag{5}$$

and $\psi(x)$ is the mother wavelet which is denoted as $\phi(x)$ in (8). In order to reconstruct a signal from its wavelet transform, we define the inverse wavelet transform as

$$f(x) = \int_{-\infty}^{\infty}\int_{0}^{\infty} F(s,u)\psi_s(x-u)dsdu \tag{6}$$

A more practical transform for numerical applications is the Discrete Wavelet Transform(DWT) which acts on a sequence of samples. In order to cover the phase-space, we need to uniformly sample the translation parameter while

exponentially sampling the scale parameter[1]. The resulting DWT is given

$$W_D[f(j,n)] = \int_{-\infty}^{\infty} f(x)\psi_{2^j}(u - n\alpha^{-j})dx \tag{7}$$

where α is the elementary dilation step. The signal may be reconstructed from its DWT by the series

$$f(x) = \sum_j \sum_n < f(u), \psi_{2^j}(u - n\alpha^{-j}) > \psi_{2^j}(u - n\alpha^{-j}) \tag{8}$$

with $< \cdot, \cdot >$ denoting the standard inner product. In practice, we choose $\alpha = 2$ for historical reasons although this is not necessary.

The Fourier transform is recognized as a transformation from the spatial domain to the wavenumber domain. However, the wavelet transform is a transformation from the spatial domain to the scale domain. This is the heart of the multiresolution interpretation of (7) as well as its fast implementation, the Fast Wavelet Transform(FWT). Each successive coefficient of the DWT describes the difference or details between the current level and a the previous decimated level. Figure 3 illustrates this concept. The first level, figure 3a, describes the smooth component of the signal. Each successive level adds detail to the reconstruction. Thus a smooth signal will have a large large-scale component and very small detail components which results in signal compaction. The efficiency of the FWT algorithm follows from the pyramid structure shown in figure 3. The highest detailed level (smallest-scale) requires that all samples be used in its computation. However each successive level requires half ($\alpha = 2$) the number of samples due to dilation which results in the FWT having the same order of operations as the FFT.

Mallat[2] was the first to recognize that this property naturally satisfies the procedure used in pyramid-encoding schemes. If one applies a two-dimensional FWT which is computed in a manner similar to the most common implementation of the two-dimensional FFT to an image, the image can be compressed into few large components and many components which are less than some tolerance whose omission does not adversely affect the fidelity of the image. Significant compression can occur depending on which analyzing wavelet is used.

We realized that the typical impedance matrix generated by a MoM code may be thought of as a complex-valued image! Thus it is reasonable to assume that we may apply the wavelet transform to a dense impedance matrix

to generate a sparse matrix. It should be mentioned that this technique is similar in concept to the Impedance Matrix Localization(IML) method proposed by Canning[11] who uses physical arguments to generate a transformation matrix which yields a sparse matrix by using sub-domain basis functions. It is not yet apparent which method yield superior results.

Suppose one wants to solve for the E-polarized scattering from a resistive strip. The appropriate integral equation is a Fredholm equation of the Second Kind

$$E_z^i(x,y) = R(x,y)J_z(x,y) + \frac{k_o}{4}\int_C J_z(x',y')H_o^{(1)}[k_o|\sqrt{(x-x')^2+(y-y'|)^2}]dl' \quad (9)$$

This may be solved numerically by converting the integral operator into a matrix operator via MoM to form the matrix equation

$$\mathbf{Z}J_z = E_z^i \quad (10)$$

where each entry of J_z and E_z^i corresponds to a spatial sample. If we look at the impedance matrix, $\mathbf{Z}$, typically it is dense. This is shown in figure 4 which is the impedance matrix generated by pulse basis-point matching on a 1λx1λ corner reflector where clearly all elements of this matrix are important.

If however we apply a wavelet transform to both sides of (10), we get the transformed equation in the scale-domain

$$\mathcal{Z}\mathcal{J}_z = \mathcal{E}_z^i \quad (11)$$

Figure 5 illustrates the matrix shown in figure 4 after wavelet transformation by the DAUB10 analyzing wavelet. Clearly, this matrix has fewer significant entries and is thus a sparse matrix. For images, edges tend to be very important thus we would use very compact (low-order) wavelets in order preserve these edges. However, when one has a smooth matrix such as the one shown in figure 4, smooth wavelets (large-order) will tend to have greater compaction capability than a small-order wavelet. In order to verify this claim, we looked at the compression realized by using different wavelets from the Daubechies family and a truncation tolerance of 10^{-2}. Table 1 summarizes the results of this study for the corner reflector when the matrix size was 32x32. We observe that the apparent storage was reduced to $\mathcal{O}$(20N) from N^2 without loss of fidelity as shown in figure 6. However, the large-order wavelets did not exhibit a significant advantage with respect to the small-order wavelets.

The reason for this unexpected result is the fact that the matrix in question is not large. A similar comparison is shown in table 2 for the case of a 6λ curved(inclusion angle = 45°) metallic strip which used a 128x128 impedance matrix. We recognize some advantage using large-order wavelets while maintaining fidelity as seen in figure 7. As a final example, we look at the simulation of a metallic half plane-linearly tapered resistive half plane junction which used a 1024x1024 matrix. A clear advantage using large-order wavelets is seen in table 3 where the apparent storage is reduced to $\mathcal{O}(70N)$ which results in a 93% storage savings without loss of fidelity as shown in figure 8!

The astute engineer will recognize the use of the term "apparent" in the preceding storage analysis. This is due to the fact that you need to generate the entire impedance matrix before transformation which results in $\mathcal{O}(N^2)$ storage. However, we have devised a simple block-by-block technique which will result in an actual memory savings. If one writes (10) as an augmented matrix equation where there are $(N/K)^2$ blocks of K^2 elements each where K is of course a power of two($\alpha = 2$) then we may write (11) as

$$\sum_{k=1}^{N/K} \mathcal{Z}_{lk}\mathcal{J}_k \;=\; \mathcal{E}_l \quad l = 1..N/K \tag{12}$$

To illustrate this technique, we looked at the junction simulation previously given. Table 4 compares the compression results realized when $K = 64$ and the tolerance was set at 10^{-4}. The total storage requirement is $K^2+\mathcal{O}(240N)$ which is a 75% storage savings compared to the original dense matrix. The degraded performance is due to that the fact that each block will require a large smooth component as well as detail components which are a result of the artificial boundaries created by the block method. It should be stressed that in spite of these artificial high components, fidelity is maintained as shown in figure 9. These observations are shown by comparing figure 10 and 11 which is the impedance matrix of a 4λ flat strip when the DAUB10 wavelet transform is applied on the entire matrix and in a block-by-block fashion with sixteen 32x32 blocks, respectively.

4 Integral Equations

The matrix compression technique described in the previous section is a rather indirect use of wavelets in electromagnetics. In this section, we will look at a more direct application of wavelets for the solution of integral equations. This method will not prove to be very useful but will provide a reference for future research.

The E-polarized scattering by a metallic strip may be solved by determining the current via the integral equation

$$E_z^i(x,y) = \frac{k_o}{4}\int_C J_z(x',y')H_o^{(1)}[k_o|\sqrt{(x-x')^2+(y-y')^2}|]dl' \tag{13}$$

where the integration domain, C, suggests the parameterization

$$\begin{aligned} x &= x(t) \\ y &= y(t) \end{aligned} \tag{14}$$

Thus (13) may be written

$$E_z^i(t) = \frac{k_o}{4}\int_{C_t} J_z(t')H_o^{(1)}[k_o|r(t,t')|]dt' \tag{15}$$

and

$$r(t,t') = \sqrt{(x(t)-x(t'))^2+(y(t)-y(t'))^2} \tag{16}$$

Let us now employ the method of weighted residuals using the discrete wavelet as an entire domain weight

$$\int_{C_t} E_z^i(t)\psi_{2^j}(t-m2^{-j})dt = \frac{k_o}{4}\int_{C_t}\int_{C_t} J_z(t')H_o^{(1)}[k_o|r(t,t')|]dt'\psi_{2^j}(t-m2^{-j})dt \tag{17}$$

If we now expand the unknown current in terms of wavelet basis(8) and realize that all of the resulting integrals are DWTs, we arrive at the matrix equation

$$\mathcal{Z}\mathcal{J}_z = \mathcal{E}_z^i \tag{18}$$

where now the impedance matrix is given directly by a two-dimensional DWT of the Hankel function of (17)

$$\mathcal{Z} = \mathcal{W}_D^2[H_o^{(1)}[k_o|r(t,t')|]] \tag{19}$$

and the unknown vector is composed of modal coefficients. This solution is analogous to finding a Fourier series expansion solution if the complex exponential is used rather than the wavelet. We also note that the scattered field is computed efficiently as

$$E_z^2 \sim \sqrt{\frac{2}{\pi k_o \rho}} e^{i(k_o\rho - \frac{\pi}{4})} \sum_{n=0}^{N-1} \left[-\frac{k_o}{4} \mathcal{E}_z^i(n) \mathcal{J}(n) \right] \tag{20}$$

where the excitation is computed via the FWT

$$\mathcal{E}_k^i = \mathcal{W}_D[e^{-ik_o[cos\phi x(t) + sin\phi y(t)]}] \tag{21}$$

Figure 12 illustrates that the aforementioned formulation does recover the solution for a 1λ metallic strip when 64 coefficients are determined. This is an unfortunately large number of terms required. The usefulness of this method does not improve with problem size as seen in figure 13 where even 1024 coefficients are not sufficient to characterize a 150λ strip. The failings of this particular formulation will be discussed in the next section.

5 Conclusions and Future Work

This paper has presented several different uses for wavelets or families of basis functions for computational electromagnetics. The relevant features and characteristics of wavelets were briefly discussed. Since the scope of this paper precludes a detailed review of wavelets, we mention that Strang[9] and Daubechies[10] give excellent reviews of wavelets. Mallat[1] not only introduces a particularly useful interpretation of wavelets and the wavelet transform, he developed from this viewpoint a quite efficient Fast Wavelet Transform which rivals the FFT in speed. Mallat also served to present this field in terms which are more accessible to engineers as compared the mathematicians "flavor" given by Daubechies.

We developed a novel technique adapted from image processing for generating a sparse matrix where previously a dense matrix was required. It should be stressed that the utility of this method solely is based of the scale characteristics of the impedance matrix rather than some restrictive mathematical operation such as convolution. The block-by-block compression method proposed resulted in significant storage savings. In the future, we are interested

in improving this method with respect to the degraded performance caused by block processing. It is reasonable to anticipate some improvement since only the most readily implemented techniques and analyzing wavelets were employed for this study and we understand the cause of the degradation. However it should be pointed out that if we can approach the efficiency of the entire matrix method, the block by block technique could be used with any existing code and a sparse matrix solver to dramatically extend the size of problems which could be handled with integral equation methods regardless of the geometry shape.

The second method looked at was a direct solution of the integral equation by wavelet expansion. This proved very disappointing. It is known that a Fourier series expansion of the current requires the retention of many terms. However, it was felt that the compact support property of wavelets would result in a dramatic reduction in the number of required coefficients. Although this initial trial did not succeed, we note that the wavelets chosen were available rather than the best possible. Further study may reveal more appropriate analyzing wavelets for our purpose or perhaps higher order wavelets are required for sufficient approximation.

Another avenue of research is employing wavelet testing with sub-domain basis functions. One may think of this operation as row-only compression rather than row and column compression which would result from the two-dimensional processing as described above. However, there would be no artificial components along the rows and by inspecting figure 11 we note that a significant amount of the spurious components are along rows of the matrix. This should result in a sparse matrix due to the local support of the basis and the compact support of the weights and a particularly appealing choice of basis are the ones used by Canning[11] since this basis will aid in compression along columns of the resulting matrix. To this date, we have not investigated this method. In addition, further study of Alpert *et al*[7] may yield further insight. It is noted that [7] investigated non-oscillating kernel functions while our kernel is certainly still a matter of research.

Wavelet processing and direct solution offers a promising avenue for extending integral equation techniques to much larger structures. It is noted that all methods described herein used FWT to evaluate all the integrals in an efficient manner. Although the examples presented involved the MoM, we are interested in using these techniques when terminating a Finite Element mesh with a boundary integral. An efficient solution in terms of unknowns

may be found for arbitrarily closures. This is in contrast the few available closures if one employs the CGFFT method to solve the boundary integral.

References

[1] Stephane G. Mallat, "Multifrequency Channel Decompositions of Images and Wavelet Models," *IEEE Trans. Acoust., Speech, Signal Processing*, Vol. 37, No. 12, pp. 2091-2110, Dec. 1989.

[2] Stephane G. Mallat, "A Theory for Multiresolution Signal Decomposition: The Wavelet Representation," *IEEE Trans. Acoust., Speech, Signal Processing*, Vol. 11, No. 7, pp. 674-693, July 1989.

[3] Ingrid Daubechies, "The Wavelet Transform, Time-Frequency Localization and Signal Analysis," *IEEE Trans. Info. Theory*, Vol. 36, No. 5, pp. 961-1005, Sept. 1990.

[4] Roland Glowinski, Wayne Lawton, Michel Ravachol, and Eric Tenenbaum, "Wavelet Solution of Linear and Nonlinear Elliptic, Parabolic, and Hyperbolic Problems in One Space Dimension," *Aware Inc. Tech. Report* AD890527.1, 1989.

[5] "Wavelet Analysis and the Numerical Solution of Partial Differential Equations," *Aware Inc. Tech. Report* AD900615.2, 1990.

[6] G. Beylkin, "On the Representation of Operators in Bases of Compactly Supported Wavelets," *pre-print.*

[7] B. Alpert, G. Beylkin, R. Coifman, and V. Rokhlin, "Wavelets for the Fast Solution of Second-Kind Integral Equations," *Yale Tech. Report* YALEU/DCS/RR-837, December 1990.

[8] G. Beylkin, R. Coifman, and V. Rokhlin, "Fast Wavelet Transforms and Numerical Algorithms I," *Comm. Pure Applied Math.*, 44:141-181, 1991.

[9] Gilbert Strang, "Wavelets and Dilation Equations: A brief introduction," *SIAM Review*,31(4):614-627, 1989.

[10] Ingrid Daubechies, "Orthonormal Bases of Compactly Supported Wavelets," *Comm. Pure Applied Math.*, 41:909-996, 1988.

[11] Francis X. Canning, "The Impedance Matrix Localization(IML) Method for Moment-Method Calculations," *IEEE Antennas and Propagat. Magazine*, pp. 18-30, October 1990.

Table 1

1 lambda Corner Reflector using 32 Unknowns and tol=10^-2

Wavelet	Zeros	Non-zeros	Total	Order
DAUB4	370	654	1024	20N
DAUB6	451	573	1024	20N
DAUB8	454	570	1024	20N
DAUB10	444	580	1024	20N
DAUB12	439	585	1024	20N
DAUB14	436	588	1024	20N
DAUB16	426	598	1024	20N
DAUB18	420	604	1024	20N
DAUB20	387	637	1024	20N

Table 2

6 lambda Curved Strip using 128 unknowns and tol=10^-2

Wavelet	Zeros	Non-zeros	Total	Order
DAUB4	10311	6073	16384	50N
DAUB6	12312	4072	16384	30N
DAUB8	13214	3170	16384	20N
DAUB10	13388	2996	16384	20N
DAUB12	13597	2787	16384	20N
DAUB14	13591	2793	16384	20N
DAUB16	13643	2741	16384	20N
DAUB18	13713	2671	16384	20N
DAUB20	13656	2728	16384	20N

Table 3

Resistive Junction using 1024 unknowns and tol=10^-4

Wavelet	Zeros	Non-zeros	Total	Order
DAUB4	573834	474742	1048576	460N
DAUB6	777806	270770	1048576	260N
DAUB8	871382	177194	1048576	170N
DAUB10	917716	130860	1048576	130N
DAUB12	940642	107934	1048576	110N
DAUB14	954802	93774	1048576	90N
DAUB16	966321	82255	1048576	80N
DAUB18	973085	75491	1048576	70N
DAUB20	978972	69604	1048576	70N

Tabel 4

Resistive Junction using block method w/ block size=64x64

Wavelet	Zeros	Non-zeros	Total	Order
DAUB4	268401	780175	1048576	760N
DAUB6	432037	616539	1048576	600N
DAUB8	569457	479119	1048576	470N
DAUB10	685377	363199	1048576	350N
DAUB12	744733	303843	1048576	300N
DAUB14	786832	261744	1048576	260N
DAUB16	796331	252245	1048576	250N
DAUB18	797724	250852	1048576	240N
DAUB20	799690	248886	1048576	240N

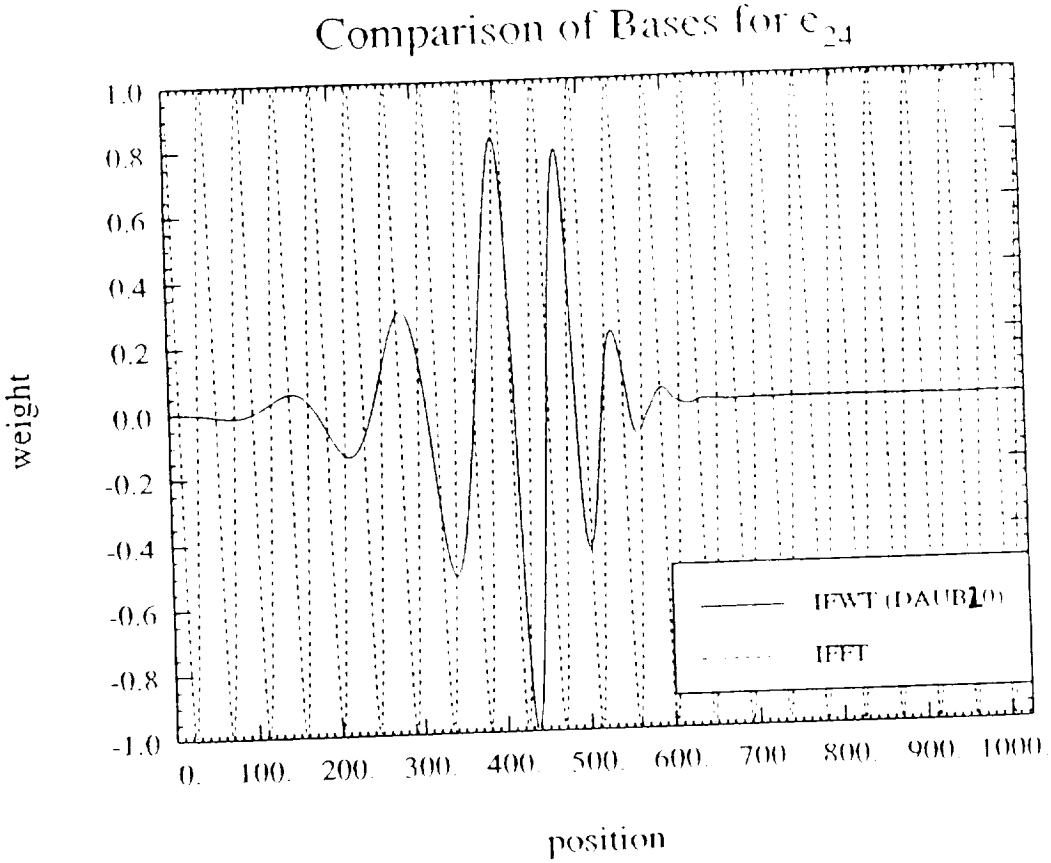
Comparison of Bases for e_{24}
weight
position
1.0
0.8
0.6
0.4
0.2
0.0
-0.2
-0.4
-0.6
-0.8
-1.0
0.
100.
200.
300.
400.
500.
600.
700.
800.
900.
1000.
IFWT (DAUB10)
IFFT

Figure 1

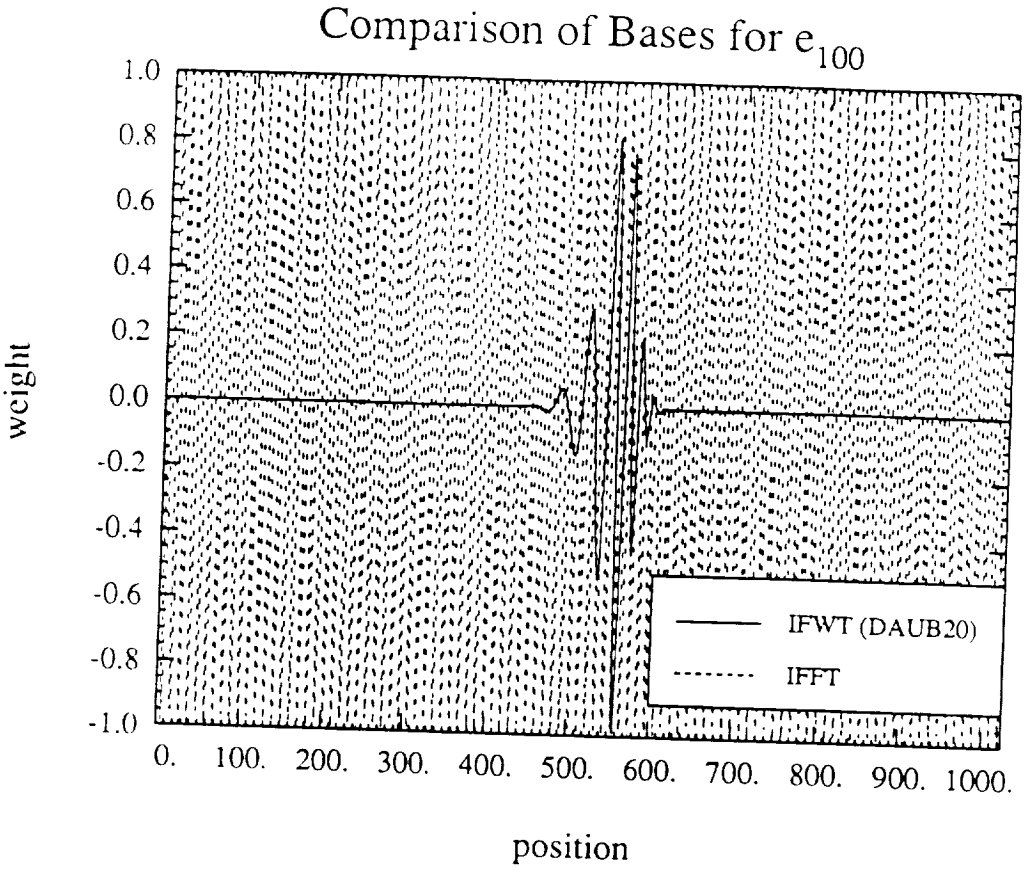
Comparison of Bases for e_{100}
1.0
0.8
0.6
0.4
0.2
0.0
-0.2
-0.4
-0.6
-0.8
-1.0
weight
0.
100.
200.
300.
400.
500.
600.
700.
800.
900.
1000.
position
IFWT (DAUB20)
IFFT

Figure 2

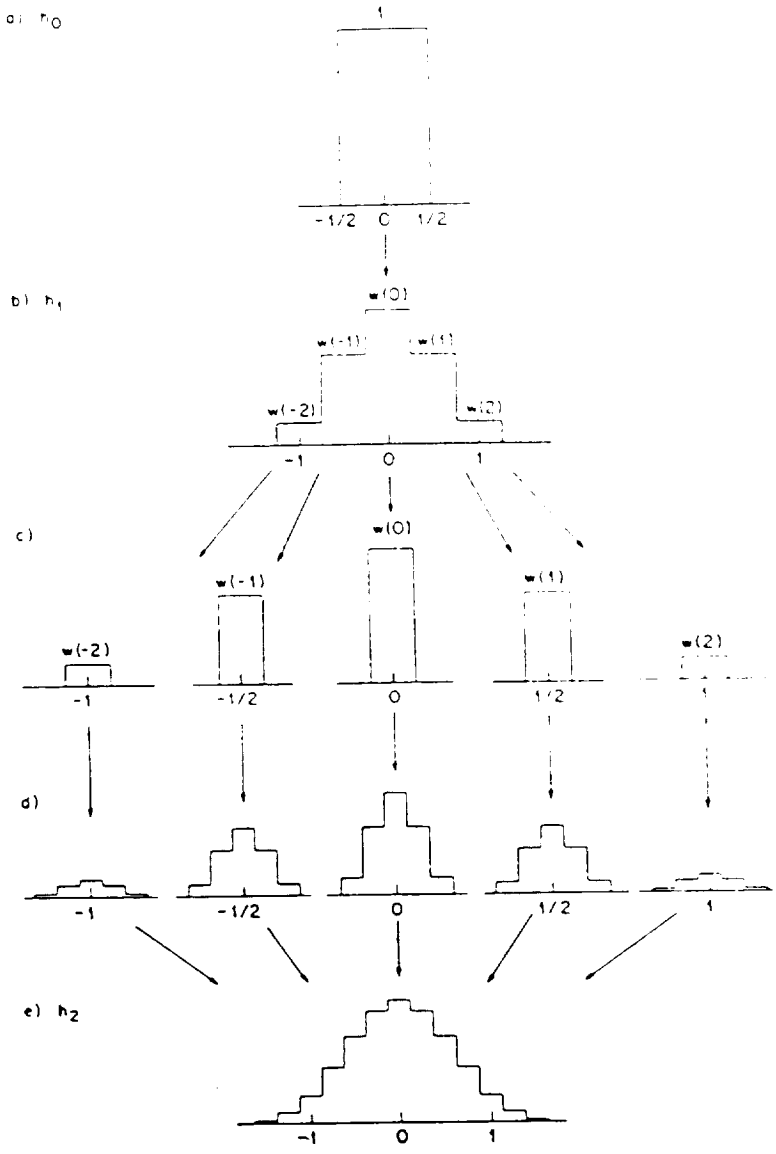

Figure 3. a) $h_0(x) = \chi_{[-1/2,1/2]}(x)$.

b) $h_1(x) = 2\sum w(n)\chi_{[n/2-1/4,n/2+1/4]}(x)$.

c) h_1 is decomposed into its "components"; each component is a multiple of the characteristic function of an interval of length $\frac{1}{2}$. (The "components" of h_j would have width 2^{-j}.)

d) Each "component" is replaced by a proportional version of h_1, centered around the same point as the component, and scaled down by a factor $\frac{1}{2}$. (This scaling factor would be 2^{-j} for h_j.)

e) The functions in d) are added to constitute h_2 (or h_{j+1}, if one starts from h_j in c)).

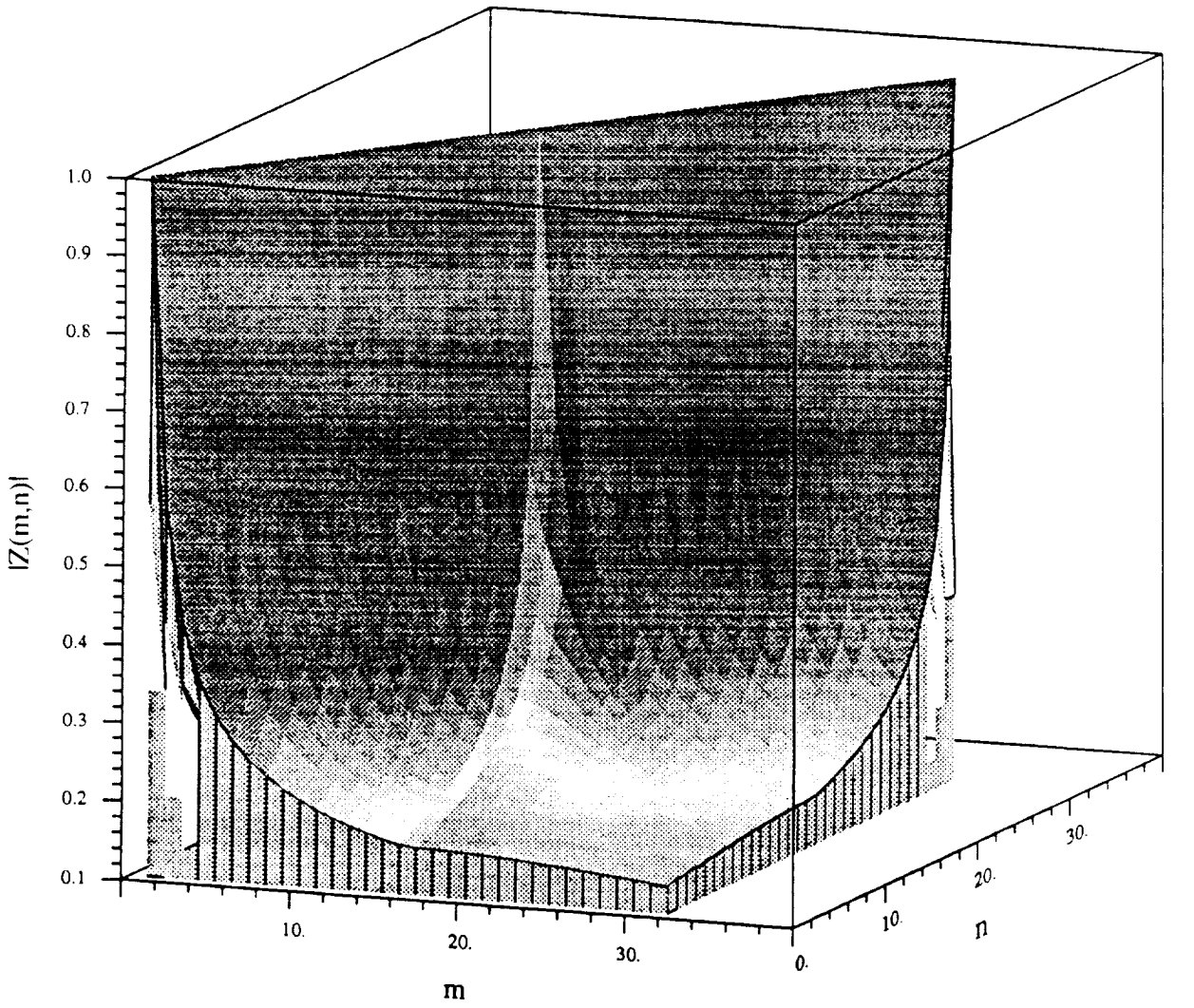
1λx1λ L-shaped Corner Reflector Impedance Matrix before Wavelet Transform
|Z(m,n)|
1.0
0.9
0.8
0.7
0.6
0.5
0.4
0.3
0.2
0.1
10.
20.
30.
m
0.
10.
20.
30.
n

Figure 4

1λx1λ L-shaped Corner Reflector Impedance Matrix after DAUB10 Wavelet Transform

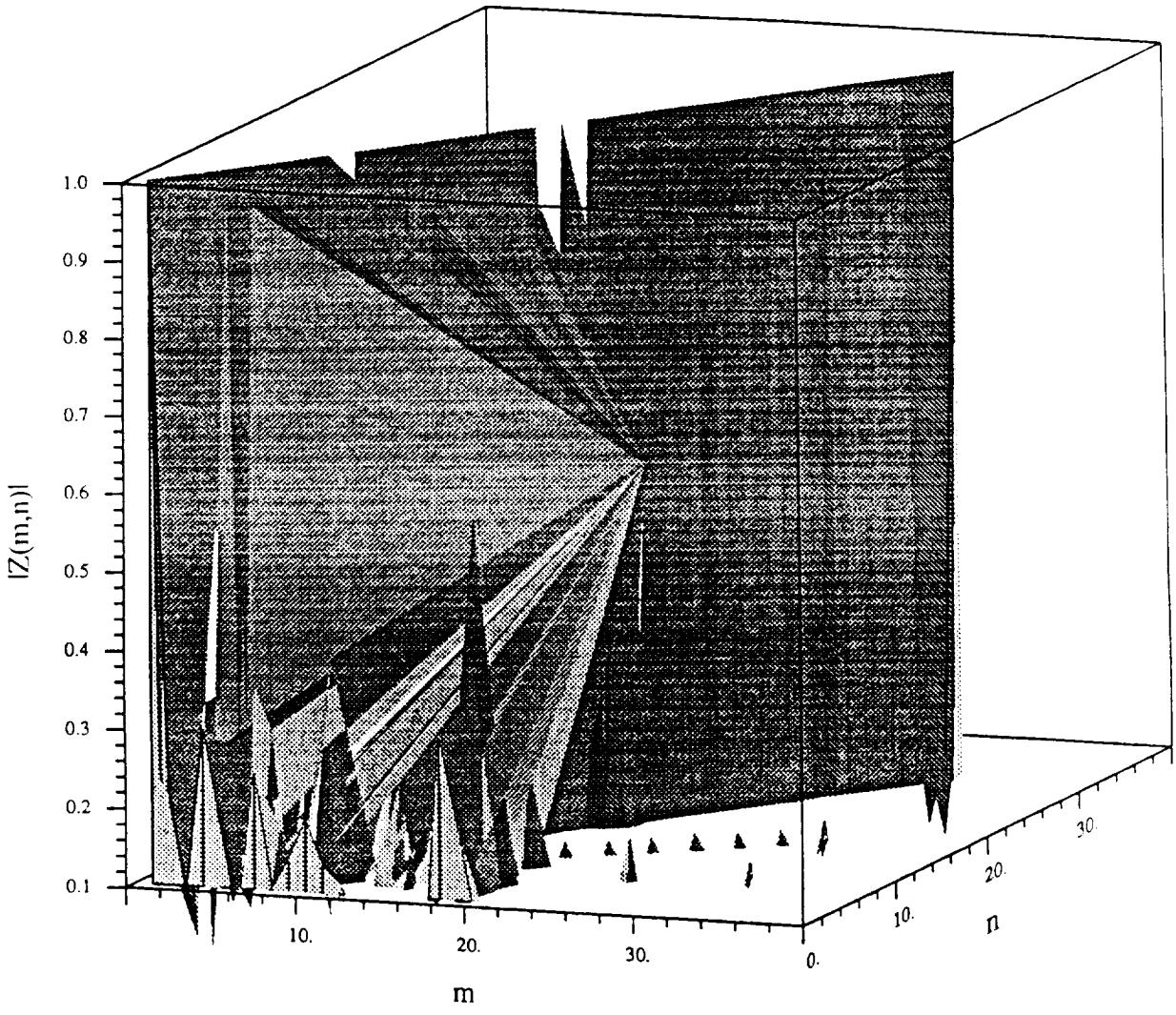

Figure 5

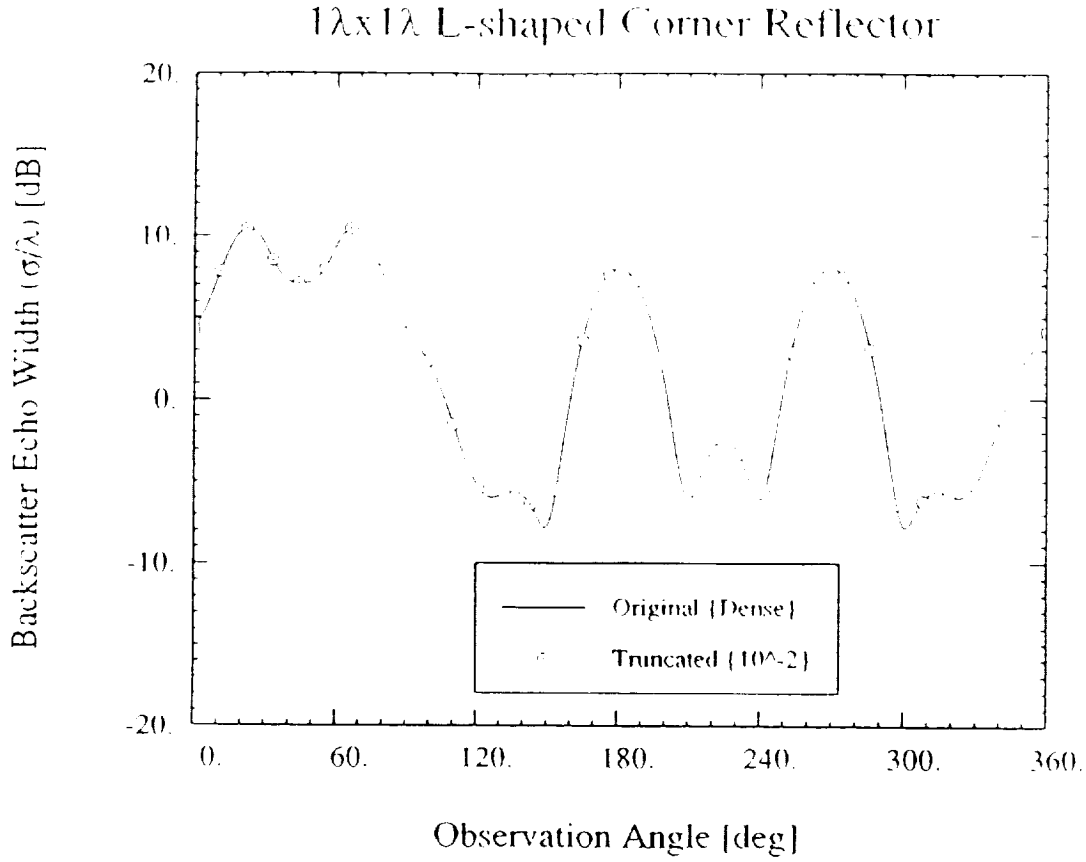
1λx1λ L-shaped Corner Reflector
Backscatter Echo Width (σ/λ) [dB]
20.
10.
0.
-10.
-20.
0.
60.
120.
180.
240.
300.
360.
Original (Dense)
Truncated (10^-2)
Observation Angle [deg]

Figure 6

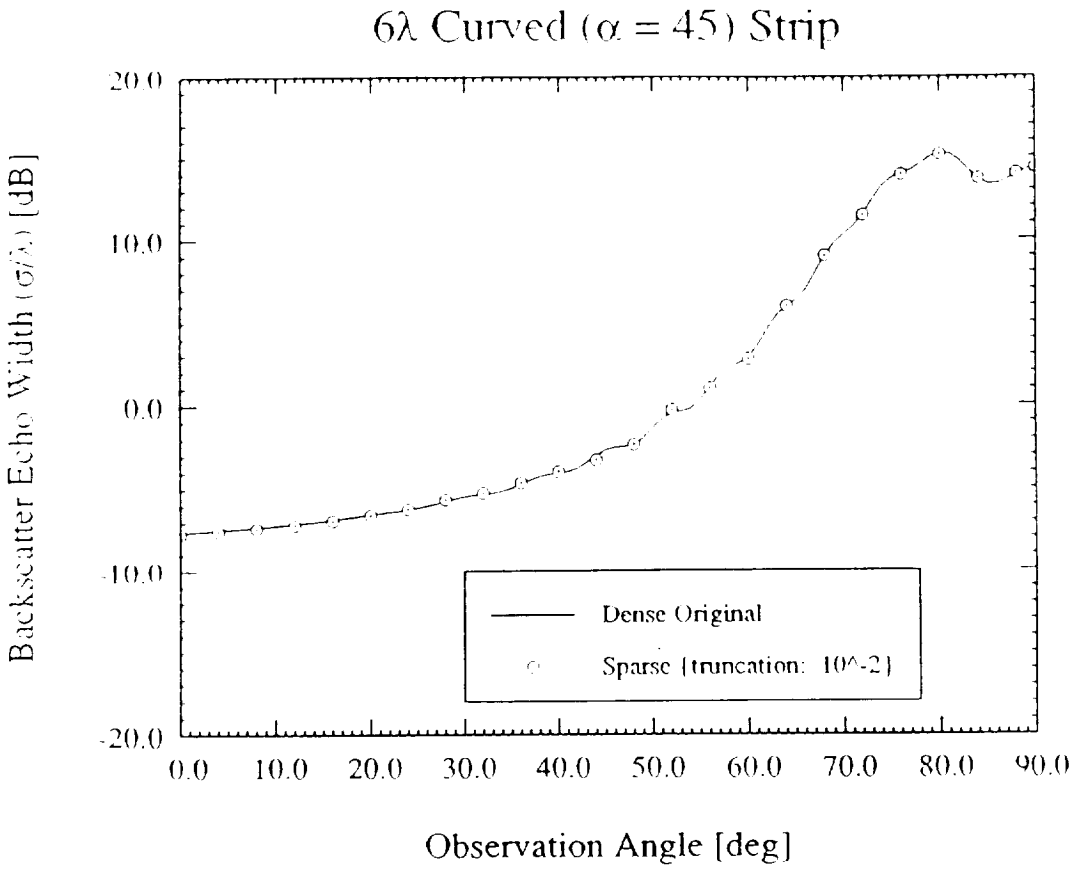
6λ Curved (α = 45) Strip
Backscatter Echo Width (σ/λ) [dB]
20.0
10.0
0.0
-10.0
-20.0
0.0
10.0
20.0
30.0
40.0
50.0
60.0
70.0
80.0
90.0
Dense Original
Sparse (truncation: 10^-2)
Observation Angle [deg]

Figure 7

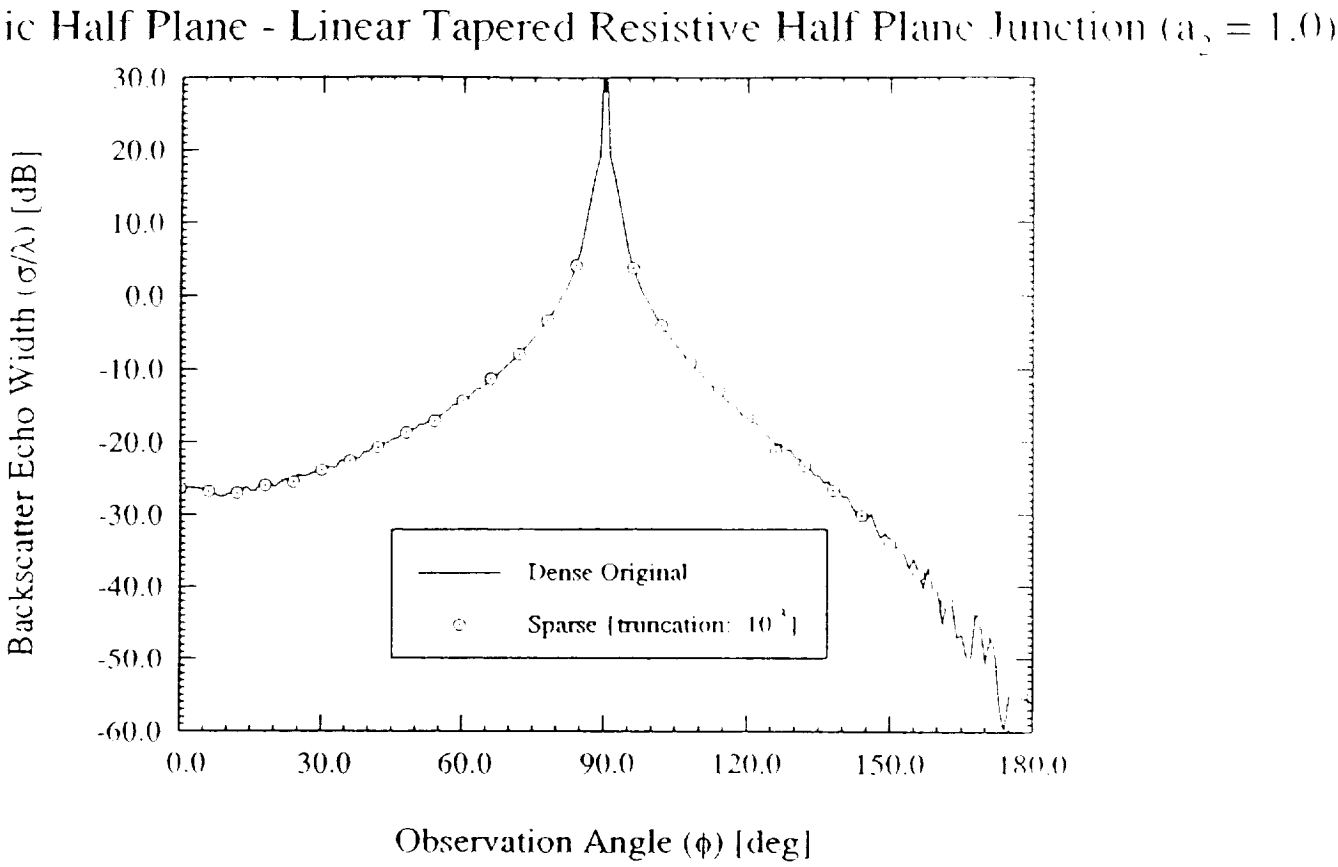
Metallic Half Plane - Linear Tapered Resistive Half Plane Junction (a_s = 1.0)
Backscatter Echo Width (σ/λ) [dB]
30.0
20.0
10.0
0.0
-10.0
-20.0
-30.0
-40.0
-50.0
-60.0
0.0
30.0
60.0
90.0
120.0
150.0
180.0
Dense Original
Sparse [truncation: 10^{-4}]
Observation Angle (ϕ) [deg]

Figure 8

:tallic Half Plane - Linear Tapered Resistive Half Plane Junction ($a_2 = 1.0$)

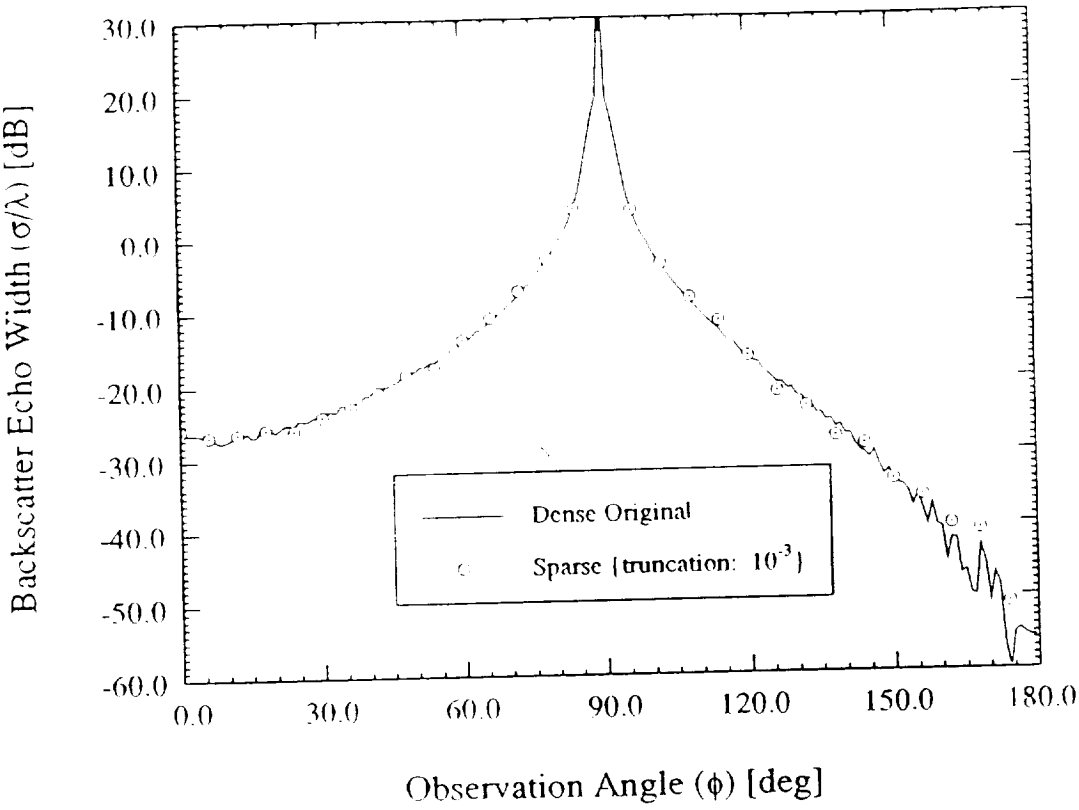

Figure 9

4λ Strip Impedance Matrix after Wavelet Transform performed all at once

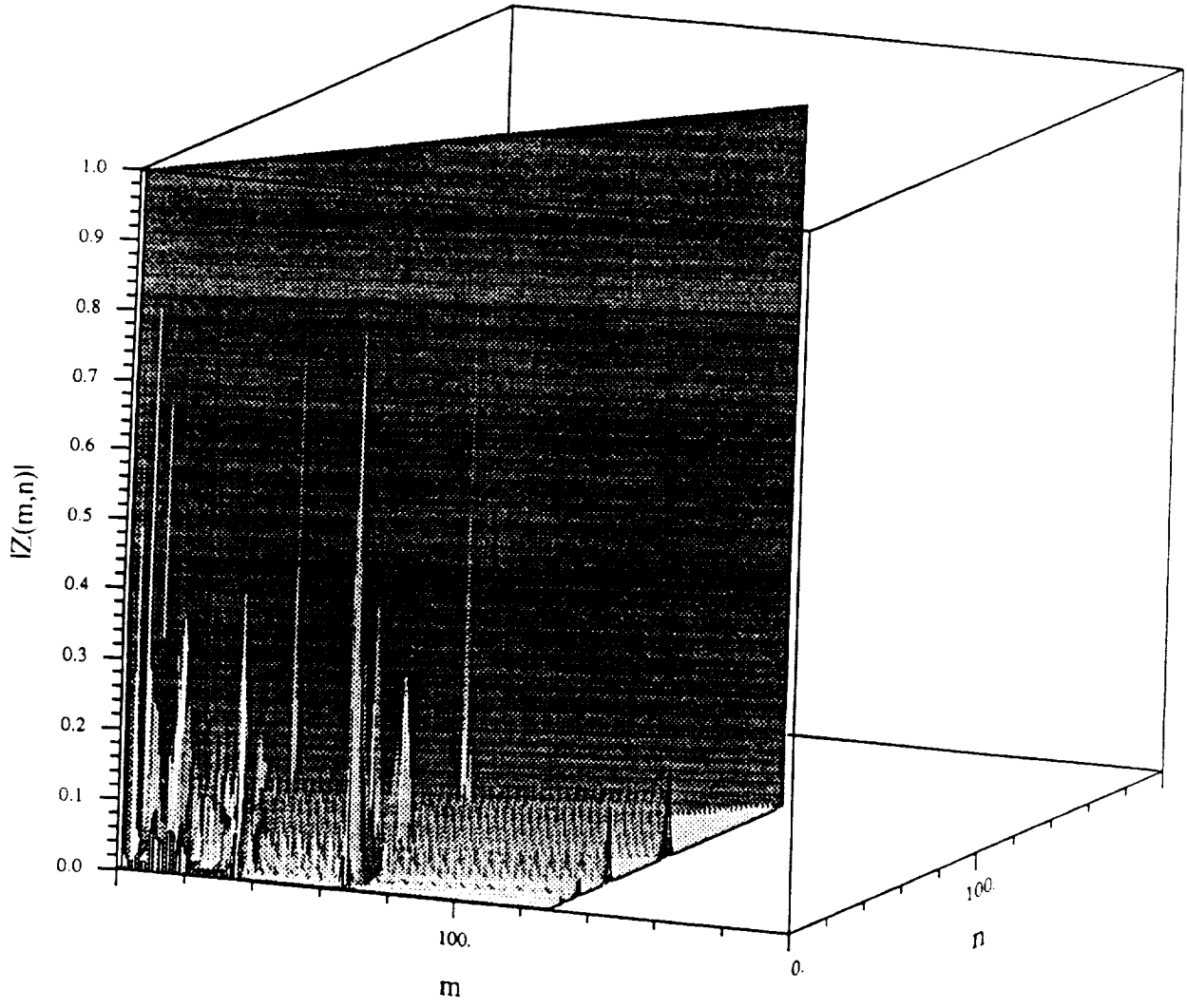

Figure 10

4λ Strip Impedance Matrix after Wavelet Transform performed block-by-block

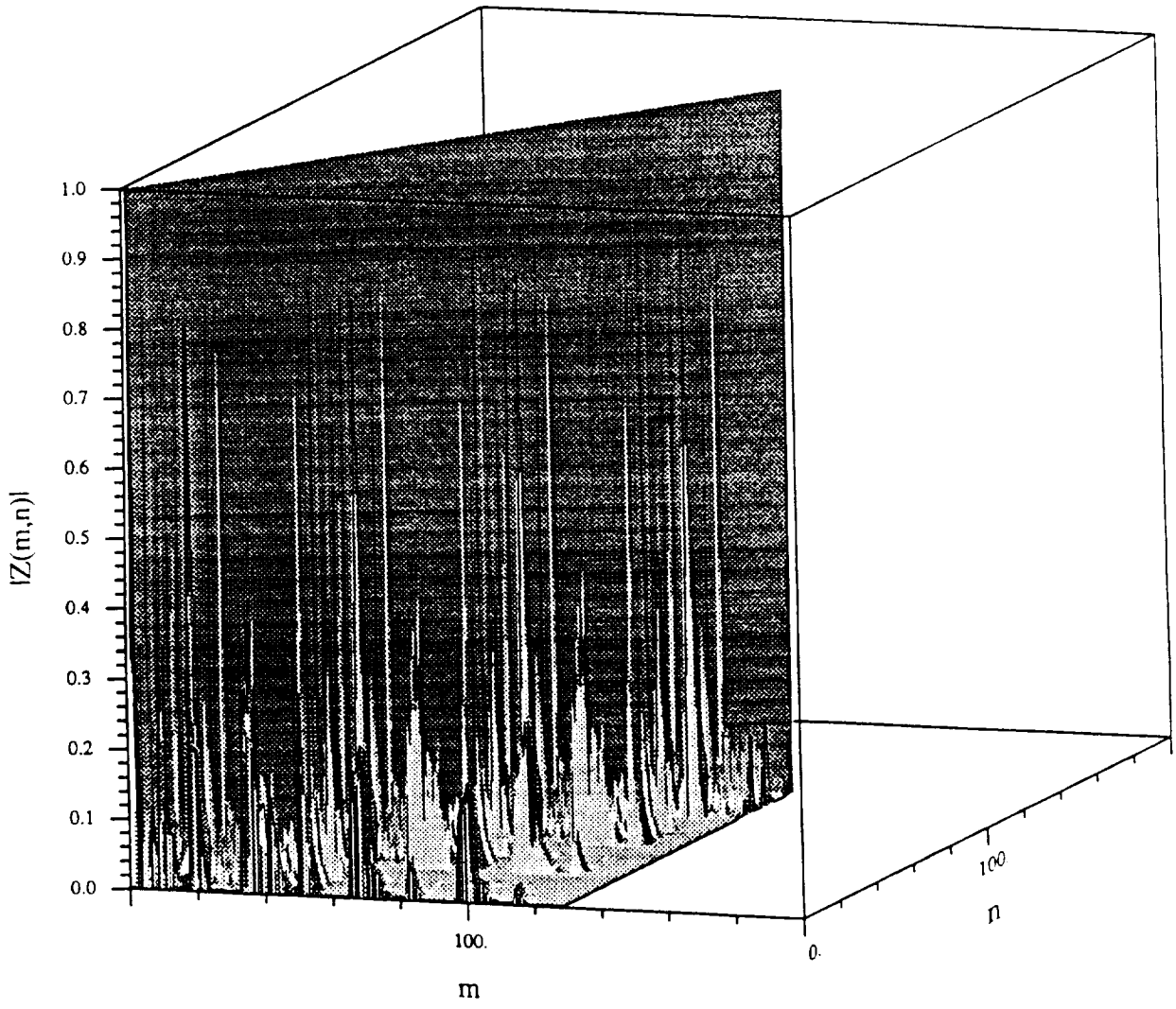

Figure 11

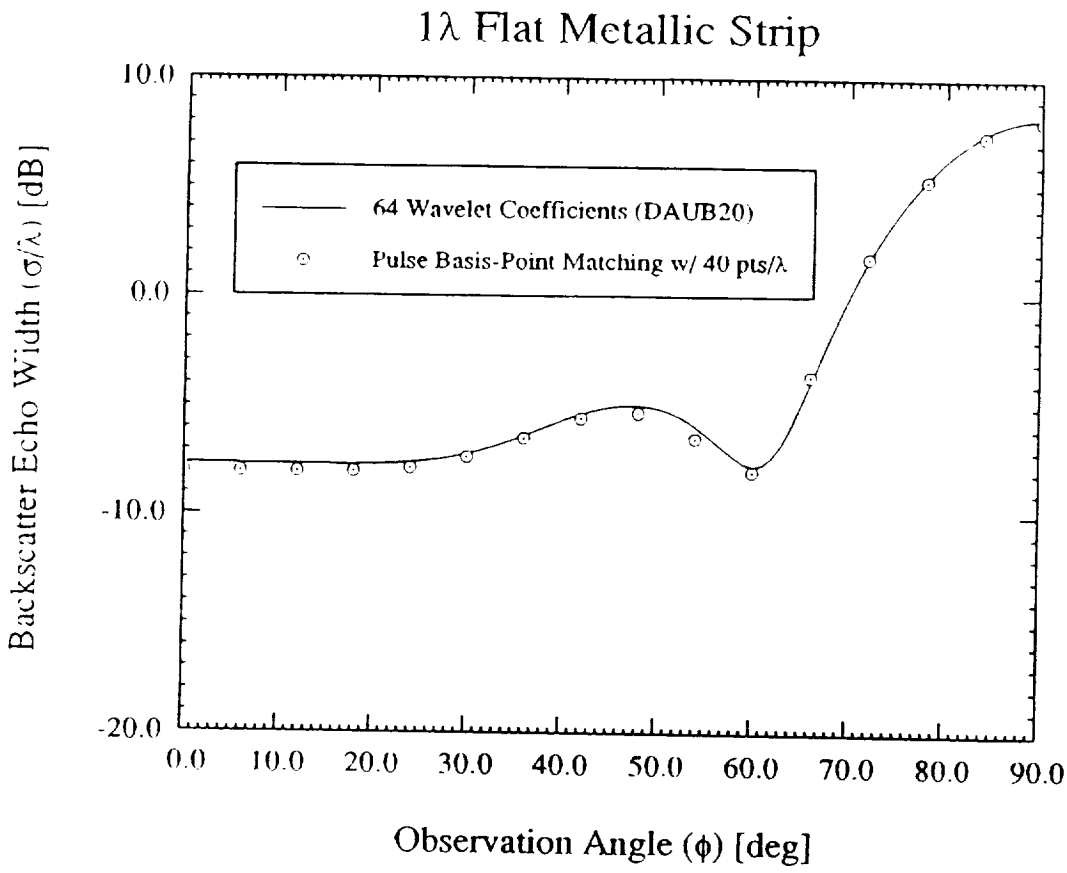
1λ Flat Metallic Strip
Backscatter Echo Width (σ/λ) [dB]
10.0
0.0
-10.0
-20.0
64 Wavelet Coefficients (DAUB20)
Pulse Basis-Point Matching w/ 40 pts/λ
0.0
10.0
20.0
30.0
40.0
50.0
60.0
70.0
80.0
90.0
Observation Angle (ϕ) [deg]

Figure 12

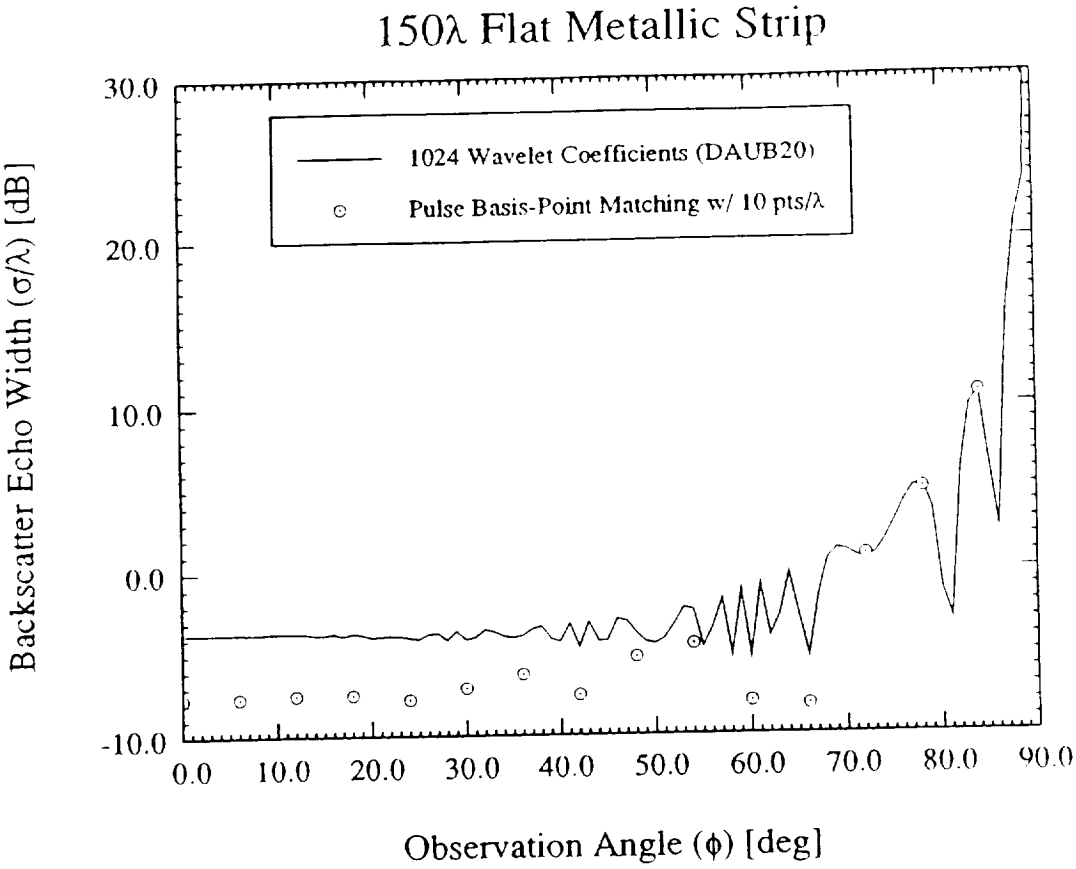
150λ Flat Metallic Strip
1024 Wavelet Coefficients (DAUB20)
Pulse Basis-Point Matching w/ 10 pts/λ
Backscatter Echo Width (σ/λ) [dB]
30.0
20.0
10.0
0.0
-10.0
0.0
10.0
20.0
30.0
40.0
50.0
60.0
70.0
80.0
90.0
Observation Angle (ϕ) [deg]

Figure 13